


RESEARCH ARTICLE

Open Access



Lipases are differentially regulated by hormones to maintain free fatty acid homeostasis for insect brain development

Yan-Xue Li^{1†}, Qiao Yan^{1†}, Tian-Wen Liu¹, Jin-Xing Wang¹ and Xiao-Fan Zhao^{1*} 

Abstract

Background Free fatty acids (FFAs) play vital roles as energy sources and substrates in organisms; however, the molecular mechanism regulating the homeostasis of FFA levels in various circumstances, such as feeding and nonfeeding stages, is not fully clarified. Holometabolous insects digest dietary triglycerides (TAGs) during larval feeding stages and degrade stored TAGs in the fat body during metamorphosis after feeding cessation, which presents a suitable model for this study.

Results This study reported that two lipases are differentially regulated by hormones to maintain the homeostasis of FFA levels during the feeding and nonfeeding stages using the lepidopteran insect cotton bollworm *Helicoverpa armigera* as a model. Lipase member H-A-like (*Lha-like*), related to human pancreatic lipase (PTL), was abundantly expressed in the midgut during the feeding stage, while the monoacylglycerol lipase ABHD12-like (*Abhd12-like*), related to human monoacylglycerol lipase (MGL), was abundantly expressed in the fat body during the nonfeeding stage. *Lha-like* was upregulated by juvenile hormone (JH) via the JH intracellular receptor methoprene-tolerant 1 (MET1), and *Abhd12-like* was upregulated by 20-hydroxyecdysone (20E) via forkhead box O (FOXO) transcription factor. Knockdown of *Lha-like* decreased FFA levels in the hemolymph and reduced TAG levels in the fat body. Moreover, lipid droplets (LDs) were small, the brain morphology was abnormal, the size of the brain was small, and the larvae showed the phenotype of delayed pupation, small pupae, and delayed tissue remodeling. Knockdown of *Abhd12-like* decreased FFA levels in the hemolymph; however, TAG levels increased in the fat body, and LDs remained large. The development of the brain was arrested at the larval stage, and the larvae showed a delayed pupation phenotype and delayed tissue remodeling.

Conclusions The differential regulation of lipases expression by different hormones determines FFAs homeostasis and different TAG levels in the fat body during the feeding larval growth and nonfeeding stages of metamorphosis in the insect. The homeostasis of FFAs supports insect growth, brain development, and metamorphosis.

Keywords Juvenile hormone, 20-Hydroxyecdysone, Lipase, Methoprene-tolerant 1, Forkhead box O

Background

Lipids are essential compounds in organisms that play important roles in energy storage, cell membrane composition, and signal transmission [1]. Triglycerides (TAGs) are a type of lipid that stores energy [2]. Fatty acids (FAs) are usually present in organisms as three primary esters: triglycerides, phospholipids, and cholesterol esters. When FAs in the circulating plasma are

[†]Yan-Xue Li and Qiao Yan contributed equally to this work.

*Correspondence:

Xiao-Fan Zhao
xfzhao@sdu.edu.cn

¹ Shandong Provincial Key Laboratory of Animal Cells and Developmental Biology, School of Life Sciences, Shandong University, Qingdao 266237, China



not present in their ester form, these FAs are called non-esterified FAs (NEFAs) or free fatty acids (FFAs). Since FAs are insoluble in water, they are transported by binding to plasma proteins. FFAs always bind to transporter proteins [3]. FFAs in animals mainly come from the digestion of dietary TAGs. The hydrolysis of dietary TAGs to FFAs is primarily triggered by pancreatic lipase (PTL) in the intestine [4]. FFAs are absorbed by intestinal cells and reassembled into DAGs or TAGs [5]. In *Drosophila* and other insects, lipoprotein-bound DAGs are circulated, and TAGs are stored in lipid droplets (LDs) [6, 7]. FFAs are an important energy source, as they undergo β -oxidation to produce ATP for the muscle, liver, heart, and other tissues [8]. The development of the brain requires a vast amount of energy, and the β -oxidation of FAs in glial cells produces metabolites that can meet approximately 20% of the neural energy requirements in the mammalian brain [9]. Excess FFAs can be esterified with glycerol into TAG and stored in fat cells in the form of LDs [10] and esterified with free cholesterol into cholesterol esters [11]. When starvation or long-term exercise occurs, lipases in adipocytes break down TAGs and release FFAs to maintain FFA homeostasis in the body [12].

Lipases are critical enzymes that degrade TAG into FAs and glycerol for energy supply during the growth and development of the body [13]. The lipase family contains a large number of members that play different roles. The major lipases of the gastrointestinal tract, such as lingual lipase (LL), gastric lipase (GL), pancreatic lipase (PTL, encoded by *Pnlip*), and pancreatic lipase-related proteins 1, 2, and 3 (PLRP), hydrolyze dietary TAGs. Lipoprotein lipase (LPL) and hepatic lipase (HL) hydrolyze vascular TAGs (lipoprotein-associated TAGs in the blood) [14]. The neutral lipases and acid lipases in lysosomes hydrolyze intracellular TAGs (TAGs stored in intracellular LDs) [13, 15]. Monoacylglycerol lipase (MGL) hydrolyzes monoacylglycerols (MAGs) in the adipose tissue [16]. The α/β -hydrolase domain-containing proteins 6 and 12 (ABHD6/12), which belong to the large α/β -hydrolase fold superfamily, hydrolyze MAG [17, 18].

The transcriptional regulation of lipase genes by hormones is the primary mechanism of lipolysis regulation. Glucocorticoids (GCs) promote pancreatic lipase (*Pnlip*) transcription to increase lipid uptake in the mouse intestine [19]. Growth hormone (GH), via signal transducer and activator of transcription 5 (STAT5), increases neutral lipase patatin-like phospholipase domain containing 2 (*Pnpla2*) transcription to promote lipolysis [20]. Adrenocorticotrophic hormone (ACTH) activates hormone-sensitive lipase/cholesterol esterase (*Lipe*) transcription to enhance the level of cholesterol needed for steroid hormone synthesis [21]. However, the regulation of FFA

homeostasis by different hormones during feeding and nonfeeding stages is not well understood.

Holometabolous insects digest dietary TAGs during larval feeding stages and degrade stored TAGs in the fat body during metamorphosis after feeding cessation, which presents a suitable model for this study. The insect midgut is responsible for food digestion, including lipid, carbohydrate, and protein absorption [22]. In the midgut, TAGs are digested by lipase to produce FFAs. FFAs are absorbed by midgut enterocyte cells for oxidation in the mitochondria or to synthesize TAGs, DAGs, and phospholipids [5]. DAGs bind to carrier proteins, are transported to peripheral storage tissues, and are subsequently stored as TAGs [7]. The insect fat body, functioning as a vertebrate liver, is a vital energy storage organ in insects and stores excess TAGs in the form of LDs during the larval feeding stage [23]. 20-Hydroxyecdysone (20E), juvenile hormone (JH), and insulin are major hormones that regulate insect development. Insulin promotes the growth and development of animals [24]. JH maintains larval status by binding to its intracellular receptor methoprene-tolerant 1 (MET1) to regulate downstream gene expression [25], while 20E antagonizes insulin and JH and promotes metamorphosis by binding to its nuclear receptor EcR to regulate downstream gene expression [26]. In *Bombyx mori*, 20E upregulates the expression of *Brummer* and *lipase-1* via forkhead box O (FOXO) transcription factor to promote lipid decomposition [27]. JH inhibits the hydrolysis of TAGs in the *Drosophila* fat body through its intracellular receptor MET [28]. Insulin inhibits FOXO activity via AKT, resulting in lipid accumulation in the *Drosophila* fat body [29]. Neuronal metabolism requires a lot of energy. In *Drosophila*, glial cells can provide metabolites to neurons through glycolysis, and FAs can be used to fuel neuronal metabolism under nutritionally restricted conditions [30, 31]. In *Helicoverpa armigera*, the FFA level is high during the feeding stage but gradually decreases during metamorphosis [32]. However, the mechanism of the homeostasis of FFA levels during larval growth and metamorphosis and its influence on brain development is not fully understood.

In the present study, we used the holometabolous insect *Helicoverpa armigera*, cotton bollworm, as a model to reveal the mechanisms of JH and 20E differentially regulate the expression of lipase member H-A-like (*Lha-like*) and the monoacylglycerol lipase ABHD12-like (*Abhd12-like*) during larval growth and metamorphosis. We revealed that *Lha-like* is upregulated in the midgut by JH via the JH intracellular receptor methoprene-tolerant 1 (MET1) during the feeding stage in larval growth, and *Abhd12-like* is upregulated in the fat body by 20E via FOXO during the nonfeeding stage in metamorphosis, thus to maintain the dynamic balance of FFA levels in

hemolymph and ensure the development of tissues at the feeding and nonfeeding stages.

Results

Classification of lipases in the *H. armigera* genome

To identify and classify the lipases of *H. armigera*, we searched for all genes in the genome of *H. armigera* by

using lipase as the keyword, and we also used lipase sequences of *B. mori*, *Drosophila melanogaster*, and *Homo sapiens* for BLAST (basic local alignment search tool) analysis in the *H. armigera* genome. A total of 83 genes encoding 97 lipase proteins were identified. A phylogenetic tree was constructed using the *H. sapiens* genome lipases as landmarks (Fig. 1). The lipases in

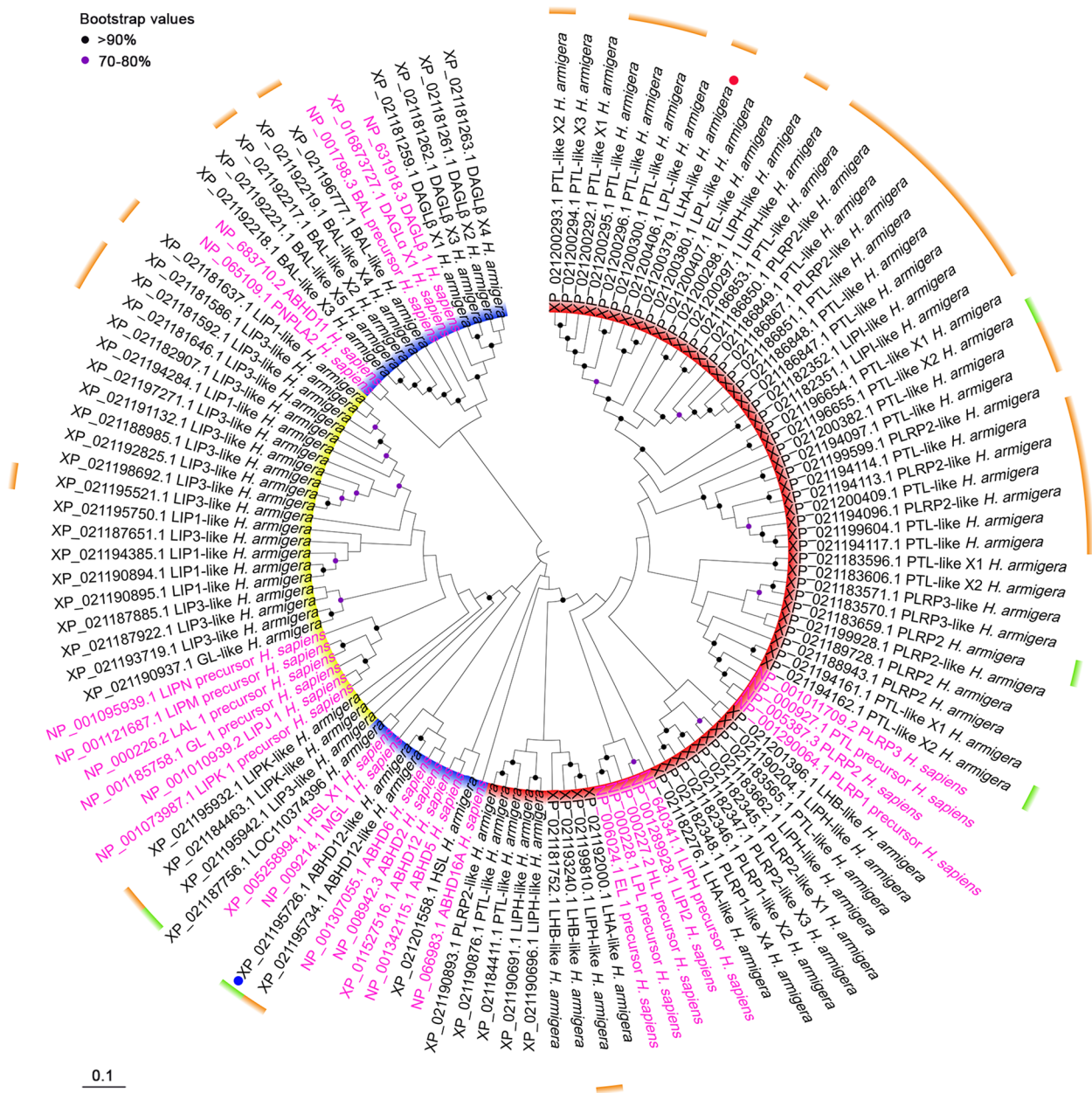


Fig. 1 Phylogenetic tree of lipases in *H. armigera*. Pink font: lipases in the *H. sapiens* genome; black font: lipases in the *H. armigera* genome. Inner red ring: lipases related to human pancreatic lipase (PTL); inner blue ring: lipases related to lipases in human adipose tissue; inner yellow ring: lipases related to human acid lipases. Outer orange ring: 32 lipases are highly expressed in the midgut at the feeding stage; outer green ring: 5 lipases are highly expressed in the fat body at the metamorphosis stage. Red dot: lipase member H-A-like (LHA-like). Blue dot: monoacylglycerol lipase ABHD12-like (ABHD12-like). The phylogenetic tree was made by MEGA 7

H. armigera were divided into three categories: the red inner ring showed that one lipase category was closely related to the human pancreatic lipase family (pancreatic lipase PTL, pancreatic lipase-related protein PLRP); the blue inner ring indicated that some of the lipases were closely related to lipases in human adipose tissue (adipose triglyceride lipase ATGL, hormone-sensitive lipase HSL, and monoacylglycerol lipase MGL); and the yellow inner ring showed that other lipases were closely related to human acid lipases (lysosomal acid lipase LAL, gastric lipase GL, lingual lipase LL). The domain of 97 proteins was predicted using the SMART tool, indicating these proteins with lipase domain, the α/β -hydrolases domain, or the patatin domain (Additional file 1: Fig. S1).

To screen the lipases that digest dietary TAG at the feeding stage and degrade fat body-stored TAG at the metamorphic stage, the transcriptome profiles of the midgut and fat body at the feeding stage (6th-24 h) and metamorphic stage (6th-96 h) were analyzed (Additional file 1: Fig. S2A). Log₂ (FPKM of 6th-24 h MG/6th-96 h MG) values greater than 2 were defined as differential expression. A total of 32 lipases were upregulated in the midgut at the feeding stage (orange outer ring in Fig. 1),

including the pancreatic lipase member H-A-like (*Lha-like*) (Additional file 1: Fig. S2B). A total of 5 lipases were upregulated in the fat body at the metamorphic stage (green outer ring in Fig. 1), including the monoacylglycerol lipase ABHD12-like (*Abhd12-like*) (Additional file 1: Fig. S2C). These results indicated that LHA-like is highly expressed during the feeding stage, and ABHD12-like is highly expressed during the metamorphic stage.

Lha-like was upregulated by JH III, while *Abhd12-like* was upregulated by 20E

To study the regulation of *Lha-like* and *Abhd12-like* expression in *H. armigera* development, the expression profiles and hormonal regulation of *Lha-like* and *Abhd12-like* were examined. *Lha-like* was expressed in the epidermis, midgut, fat body, and brain. In the midgut, the mRNA levels of *Lha-like* increased at the sixth instar feeding stage (6th-6 h to 6th-48 h) compared with the metamorphic stage (6th-72 h to 6th-120 h) (Fig. 2A), indicating that LHA-like plays an essential role during feeding stage. To understand the hormonal regulation of LHA-like, JH III was injected into the larval hemocoel. The expression of *Lha-like* in the midgut was increased

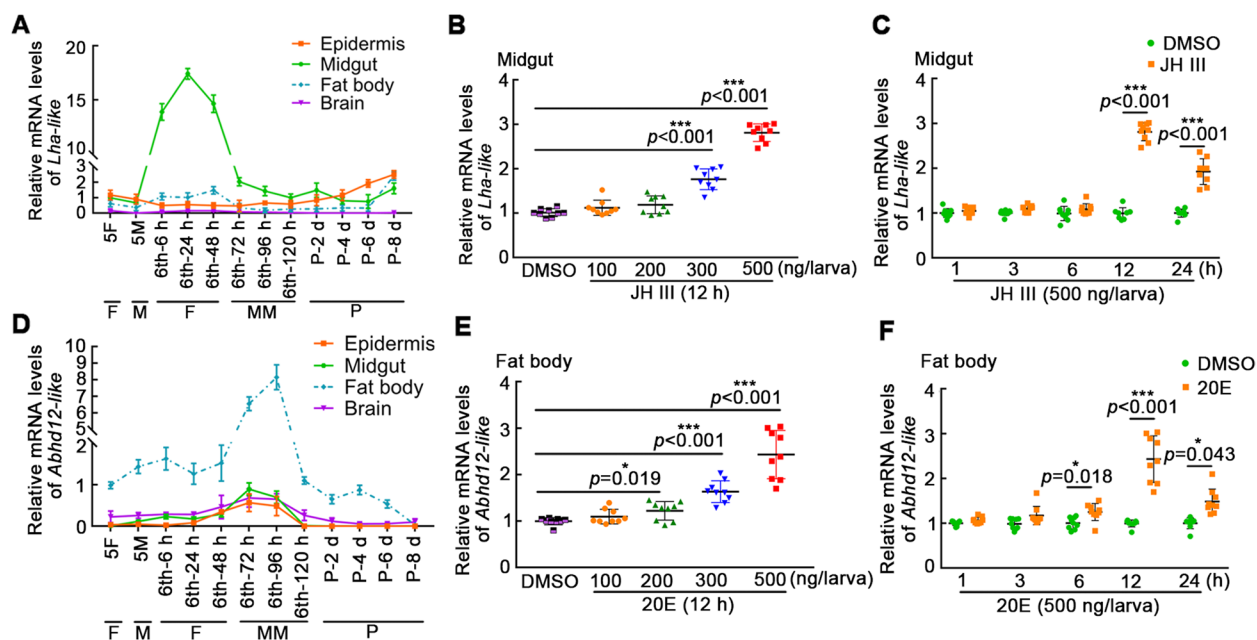


Fig. 2 The expression profiles and hormone induction of *Lha-like* and *Abhd12-like*. **A** The mRNA levels of *Lha-like* in the epidermis, midgut, fat body, and brain were measured using qRT-PCR. 5F: fifth instar feeding larvae; 5M: fifth instar molting larvae; 6th-6 h to 120 h represent sixth instar larvae at different stages. P2 to P8: 2- to 8-day-old pupae. F: feeding; M: molting; MM: metamorphosis molting; P: pupae. $n = 3$. **B** The expression of *Lha-like* in the midgut under stimulation with different concentrations of JH III for 12 h. DMSO was used as the control. $n = 9$. **C** Time course of *Lha-like* expression in the midgut after JH III (500 ng/larva) induction. $n = 9$. **D** qRT-PCR analysis of *Abhd12-like* mRNA levels in the epidermis, midgut, fat body, and brain. $n = 3$. **E** The expression of *Abhd12-like* in the fat body under stimulation with different concentrations of 20E for 12 h. DMSO was used as the control. $n = 9$. **F** Time course of *Abhd12-like* expression in the fat body after 20E (500 ng/larva) induction. $n = 9$. The error bar represents the mean \pm SD of three biological replicates. * $p < 0.05$, ** $p < 0.01$, *** $p < 0.01$ (two-tailed Student's *t* test). n indicates the number of data points and Additional file 2 for individual data values

in JH III concentration- and in a time-dependent manner (Fig. 2B and C), indicating that JH III promotes *Lha-like* expression. Lipases *Ptl-like*, *Plrp2-like*, and *Liph-like* had similar expression profiles and JH III regulation (Additional file 1: Fig. S3). *Abhd12-like* was expressed in the epidermis, midgut, fat body, and brain, and was highly expressed in the fat body. The mRNA levels of *Abhd12-like* increased at the metamorphic stage compared with the sixth instar feeding stage (Fig. 2D), indicating that ABHD12-like plays an important role during metamorphosis. The expression of *Abhd12-like* in the fat body was increased by 20E concentration- and a time-dependent manner (Fig. 2E and F), indicating that 20E promotes *Abhd12-like* expression. In addition, *Lha-like* was induced by insulin but not by 20E (Additional file 1: Fig. S4A and B), whereas *Abhd12-like* was not upregulated by JH III or insulin (Additional file 1: Fig. S4C and D). These data confirmed the differential expression of the two lipases under JH III and 20E regulation.

JH III promoted the transcription of *Lha-like* via MET1

To further explore the molecular mechanism by which JH III promotes *Lha-like* expression, the possible JH response element (JHRE) for MET1 binding in the 5' upstream sequence of *Lha-like* were predicted by a website (http://jaspar.binf.ku.dk/cgi-bin/jaspar_db.pl). There were a highly conserved sequence of JHRE, 5' ₃₇₆CCTCACGAAGTG₃₆₅3', in the 5' upstream sequence of *Lha-like* in comparison with the JHRE of the *Aedes aegypti* early trypsin gene (*Et*) [33] (Fig. 3A). After knocking down *Met1*, the expression levels of *Lha-like* decreased significantly in the midgut (Fig. 3B), suggesting that JH III upregulates the expression of *Lha-like* via MET1.

To confirm that MET1 activates the transcription of *Lha-like*, a pIEx-4-LUCI-GFP-His plasmid was constructed, and the LUCI-GFP-His reporter was shown to be overexpressed in HaEpi cells, a cell line established from the epidermal cells of *H. armigera* [34] (Additional

file 1: Fig. S5). The promoter of the pIEx-4-LUCI-GFP-His plasmid was replaced by the 5' upstream sequence of *Lha-like* (-1292~ATG) to construct the *pLha*-LUCI-GFP-His reporter plasmid and was overexpressed with the MET1-RFP-His transcription factor in HaEpi cells (Fig. 3C). Western blotting showed that in the RFP-His control, the *pLha*-LUCI-GFP-His reporter plasmid had basal expression in the DMSO control; however, JH III significantly upregulated the expression of LUCI-GFP-His compared with DMSO treatment. The basal expression of LUCI-GFP-His in the DMSO- or JH III-treated RFP-His control was derived from endogenous MET1 in the cells. When MET1-RFP-His was overexpressed, a significant increase in the expression level of LUCI-GFP-His was observed under JH III induction compared with DMSO induction (Fig. 3D). When *pLha*-LUCI-GFP-His, pRL-TK, and MET1-RFP-His were co-transfected into cells, the luciferase activity showed similar results with western blotting (Fig. 3E). A chromatin immunoprecipitation (ChIP) assay showed that MET1-RFP-His bound more JHRE in the *Lha-like* promoter under JH III treatment than it did under DMSO treatment. JH III treatment enhanced the binding intensity of MET1 to JHRE. As a label control, when RFP-His was overexpressed, the RFP-His protein could not bind to JHRE, and JHRE fragments could not be enriched under either DMSO or JH treatment (Fig. 3F), which confirmed that JH III upregulates *Lha-like* expression through MET1.

20E promoted the transcription of *Abhd12-like* via FOXO

To analyze the mechanisms by which 20E upregulated the expression of *Abhd12-like*, the binding sites of transcription factors were predicted. Two possible FOXO-binding elements (FOXOBE1 ₋₁₈₇₄ATGTTTAA₋₁₈₆₇, FOXOBE2 ₋₇₀₄TTGTTTTA₋₆₉₇) were predicted in the 5' upstream sequence of the *Abhd12-like* by the JASPAR transcription factor database. The two FOXOBE sequences in *Abhd12-like* were highly conserved with the FOXOBE sequence

(See figure on next page.)

Fig. 3 JH III upregulated the expression of *Lha-like* via MET1. **A** Alignment of JHRE of *Et* from *A. aegypti* and *Lha-like* from *H. armigera*. **B** The expression of *Lha-like* was measured after *Met1* knockdown in the midgut, followed by stimulation with JH III (500 ng/larva) for 12 h. The fifth instar 20 h larvae were injected with the dsRNA three times, 24 h apart, and JH III was injected after 12 h the third dsRNA injection. $n = 9$. **C** Schematic diagram of the *pLha*-LUCI-GFP-His reporter plasmid. **D** Western blotting showed the difference in reporter gene expression levels of *pLha*-LUCI-GFP-His under different treatments. ACTB was used as a loading control. The ratio of the reporter protein to ACTB band density was statistically calculated by ImageJ. The mRNA levels of *Met1* in HaEpi cells under different treatments were measured by qRT-PCR. Cells were incubated with 2 μ M JH III for 24 h. $n = 3$. **E** Transcriptional activity was detected by dual-luciferase reporter assay. The MET1-RFP-His or RFP-His with *pLha*-LUCI-GFP-His vector and the reference pRL-TK vector were cotransfected into HaEpi cells. The *pLha*-LUCI-GFP-His vector carries firefly luciferase. The reference pRL-TK vector carries renilla luciferase. The relative luciferase activity was defined as the reporter firefly luciferase level/the reference renilla luciferase level. Fluc: Firefly luciferase; Rluc: Renilla luciferase. $n = 3$. **F** ChIP assay showing that JH III upregulated *Lha-like* expression via MET1 binding to JHRE, as measured by qRT-PCR. Primer JHRE is the sequence containing JHRE. The primer sequence of *Lha-like* was used as a non-JHRE control targeting the *Lha-like* open reading frame (ORF). $n = 3$. The error bar represents the mean \pm SD of three biological replicates. *** $p < 0.01$ (two-tailed Student's *t* test). The comparison between multiple sets of data was analyzed by ANOVA. The different lowercase letters show significant differences. *n* indicates the number of data points and Additional file 2 for individual data values

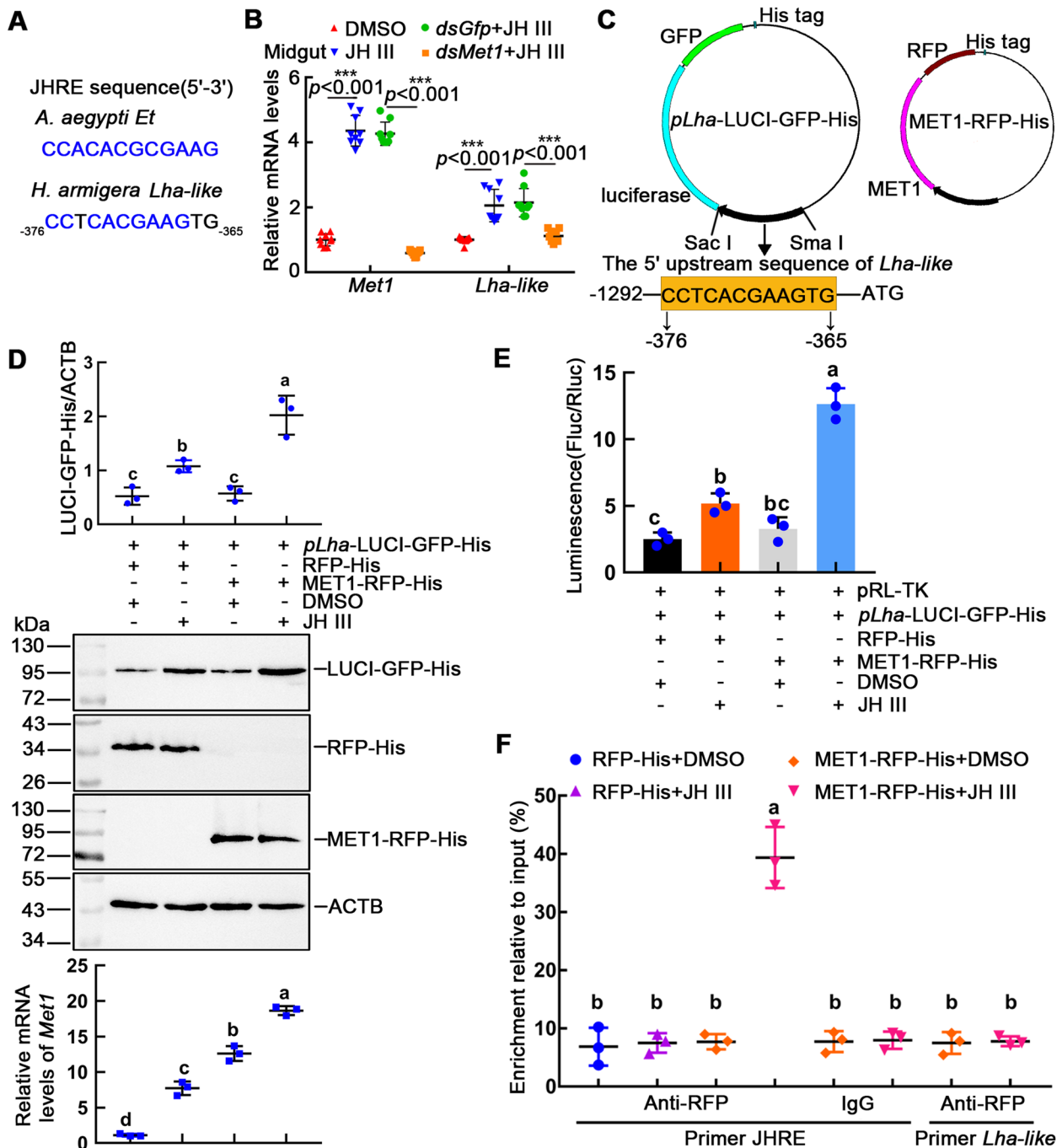


Fig. 3 (See legend on previous page.)

of *H. armigera* *Brz7* gene [35] (Fig. 4A). Interference of *Foxo* in the fat body by RNAi decreased the expression levels of *Abhd12-like* (Fig. 4B). In addition, an ecdysone response element (EcRE₋₆₂₁TCAATA₋₆₁₆) was predicted in the 5' upstream sequence of *Abhd12-like*, which was similar to the EcRE in *Hr3* [36] (Fig. 4C). Interference with *Ecr* led to a decrease in *Abhd12-like* and *Foxo*

expression levels in the fat body (Fig. 4D). These results suggested that *Abhd12-like* is upregulated by both FOXO and EcR.

To address whether *Abhd12-like* was upregulated by FOXO or EcR directly, the *pAbhd12-LUCI-GFP-His* reporter plasmid was constructed by insertion of the 5' upstream sequence of *Abhd12-like* (-2142~ATG)

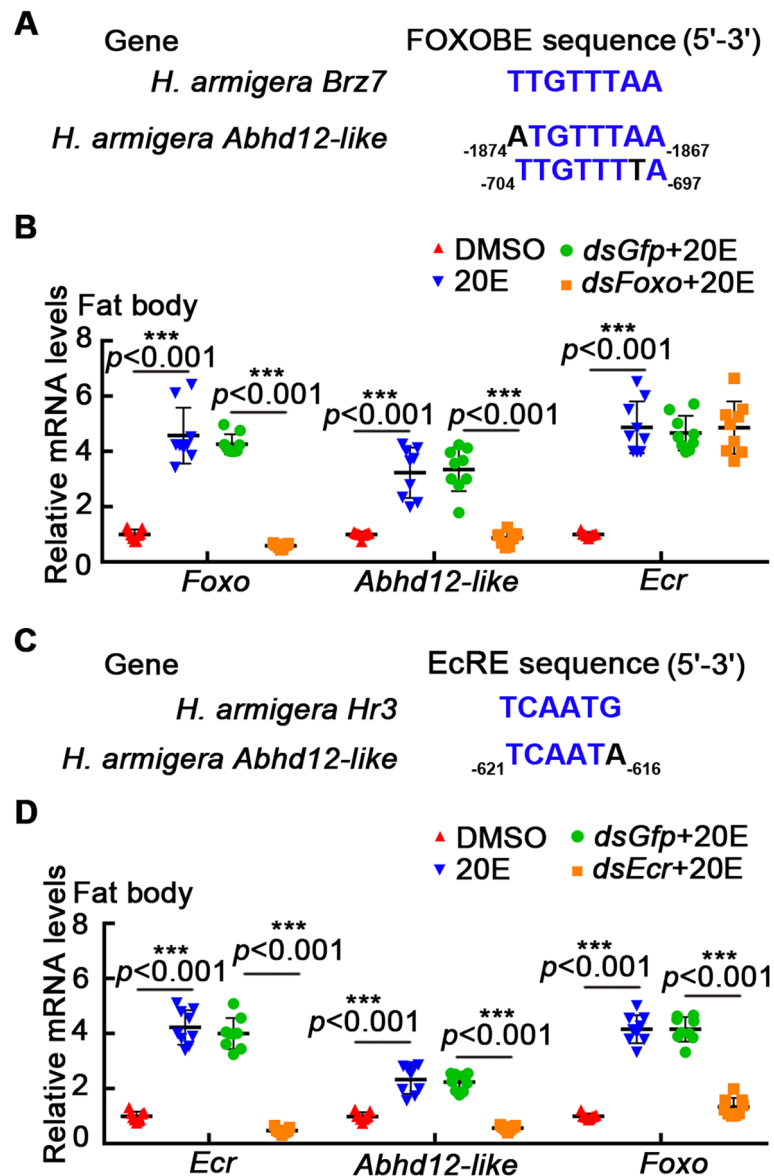


Fig. 4 EcR and FOXO were involved in 20E up-regulation of *Abhd12-like* expression. **A** Sequence alignment of FOXOBE in the 5' upstream sequence of *Brz7* and *Abhd12-like* from *H. armigera*. **B** The mRNA levels of *Abhd12-like* after knockdown of *Foxo* in the fat body. The sixth instar 6 h larvae were injected with *dsFoxo* or *dsGfp* three times at intervals of 24 h, and 20E was injected after the last dsRNA injection 12 h. **C** Sequence alignment of EcRE in the 5' upstream sequence of *Hr3* and *Abhd12-like* from *H. armigera*. **D** The mRNA levels of *Abhd12-like* after knockdown of *Ecr* in the fat body. The sixth instar 6 h larvae were injected with the dsRNA three times, 24 h apart, and 20E was injected after the third dsRNA injection 12 h. The error bar represents the mean \pm SD of three independent experiments. Statistically significant differences were calculated using two-tailed Student's *t* tests (* $p < 0.05$, ** $p < 0.01$). $n = 9$ for all graphs and see Additional file 2

and was overexpressed together with FOXO-RFP-His or EcR-RFP-His in HaEpi cells (Additional file 1: Fig. S6). When *pAbhd12-LUCI-GFP-His* was cotransfected with the RFP-His control plasmid, there was no expression of LUCI-GFP-His under DMSO treatment, while the expression of LUCI-GFP-His was induced under 20E treatment, which was caused by the endogenous FOXO induced by 20E in HaEpi cells. When

pAbhd12-LUCI-GFP-His was cotransfected with FOXO-RFP-His, no LUCI-GFP-His expression was observed under DMSO treatment, but 20E significantly induced LUCI-GFP-His expression compared to the RFP-His control plasmid, indicating that the transcriptional activity of *pAbhd12-LUCI-GFP-His* was strictly induced by 20E via FOXO (Fig. 5A). This result was confirmed by the dual-luciferase reporter assay (Fig. 5B). The binding of FOXO

to the FOXOBE in the 5'-upstream of *Abhd12-like* was verified by ChIP assay. The overexpressed FOXO-RFP-His in the HaEpi cells was confirmed to bind more FOXOBE1 fragments and FOXOBE2 fragments in promoter of *Abhd12-like* under 20E induction than under DMSO condition. 20E treatment enhanced the binding intensity of FOXO to FOXOBE. As a label control, when RFP-His was overexpressed, RFP-His protein could not bind to FOXOBE, and FOXOBE fragments could not be enriched under either DMSO or 20E treatment (Fig. 5C). These results suggested that the transcription of *Abhd12-like* is strictly regulated by 20E via FOXO.

To validate that 20E upregulated *Abhd12-like* expression via EcR, the *pAbhd12-LUCI-GFP-His* reporter plasmid and EcR-RFP-His were coexpressed in HaEpi cells. Reporter gene expression (LUCI-GFP-His) was detected by western blotting. DMSO, as the solvent control, could not induce the expression of LUCI-GFP-His; in contrast, LUCI-GFP-His was induced by 20E treatment when RFP-His was overexpressed. LUCI-RFP-His was also detected when EcR-RFP-His was overexpressed and 20E was applied. However, there was no significant difference compared to RFP-His (Fig. 5D), indicating that 20E did not directly upregulate the expression of *Abhd12-like* via EcR.

Knockdown of *Lha-like* or *Abhd12-like* caused a decrease of FFA levels in hemolymph and slowed brain development

To determine the role of *Lha-like* in insect development, we knocked down *Lha-like* by injecting *dsLha-like* into the fifth instar 20 h larval hemocoel. The mRNA levels of *Lha-like* were confirmed to be significantly decreased in the midgut (Fig. 6A). Knockdown of *Lha-like* resulted in a decrease in both the levels of FFAs in the hemolymph and TAGs in the fat body (Fig. 6B and C). Nile red staining showed that LDs of fat body cells were densely distributed in the *dsGfp* group (Fig. 6D), while the LD size was smaller in the *dsLha-like* group (Additional file 1: Fig. S7A-C). After the knockdown of *Lha-like*, the brain

morphology was abnormal, the brain size was small, and the brain development was severely delayed (Fig. 6E and F). The larvae showed delayed pupation and small pupae after knockdown of *Lha-like* (Fig. 6G). After injecting *dsLha-like*, all the larvae's average pupation time was delayed by 12 h compared with that in larvae injected with *dsGfp*, and 49% of larvae showed a significant delay in pupation for an average of 23 h (Fig. 6H and I). The 28% of larvae had a small pupae phenotype, and the average weight of pupae was decreased compared with that of larvae injected with *dsGfp* (Fig. 6J and K). In addition, in the *dsGfp* control group, the midgut showed the red color, the red color exhibited characteristics of degradation of larval midgut, whereas *dsLha-like*-treated larval midgut did not appear red (Additional file 1: Fig. S7D). Hematoxylin and eosin (HE) staining analysis further revealed that the larval midgut (LM) did not separate from the imaginal midgut (IM) in the *dsLha-like*-treated larval midgut, compared with the larvae injected with the control *dsGfp* (Additional file 1: Fig. S7E). Meanwhile, in the *dsGfp* group, the fat body began to decompose, in contrast, the fat body of *dsLha-like*-treated was intact (Additional file 1: Fig. S7F and G). The expression of *Ptl-like*, *Plrp2-like*, and *Liph-like* was detected to show that there was no off-target effect of *Lha-like* knockdown (Additional file 1: Fig. S7H). These data showed that LHA-like digests dietary TAG to produce FFAs to support larval growth, larval brain development, TAG store in fat body, and metamorphosis.

Abhd12-like was knocked down by the injection of dsRNA into the sixth instar 6 h larval hemocoel to examine its role in insect development (Fig. 7A). The level of FFAs in the hemolymph was decreased, whereas the level of TAGs in the fat body was increased (Fig. 7B and C). After the knockdown of *Abhd12-like*, LDs remained in tight distribution (Fig. 7D) and the LD size was large, compared with *dsGfp* group (Additional file 1: Fig. S8A-C). The morphology of the brain was arrested in the larval stage, and brain development was seriously hindered

(See figure on next page.)

Fig. 5 20E upregulated the expression of *Abhd12-like* via EcR and FOXO. **A** Western blotting showed the difference in protein levels of LUCI-GFP-His under different treatments, and the mRNA levels of *Foxo* in HaEpi cells under different treatments were measured by qRT-PCR. Cells were incubated with 2 μ M 20E for 24 h. **B** Transcriptional activity of the *pAbhd12-LUCI-GFP-His* reporter plasmid was detected by dual-luciferase reporter assay. The FOXO-RFP-His or RFP-His with *pAbhd12-LUCI-GFP-His* plasmid and the reference pRL-TK plasmid were cotransfected into HaEpi cells. The *pAbhd12-LUCI-GFP-His* vector carries firefly luciferase. The reference pRL-TK vector carries renilla luciferase. The relative luciferase activity was defined as the Fluc level/Rluc level. Fluc: Firefly luciferase; Rluc: Renilla luciferase. **C** ChIP assay showing that 20E promoted *Abhd12-like* expression via FOXO binding to FOXOBE, as measured by qRT-PCR. The FOXOBE1 primer is the sequence containing FOXOBE1. The FOXOBE2 primer is the sequence containing FOXOBE2. The *Abhd12-like* primer was used as a non-FOXOBE control targeting the *Abhd12-like* ORF. **D** The expression of LUCI-GFP-His was analyzed by western blotting under different conditions. ACTB was used as the loading control. Cells were incubated with 2 μ M 20E for 24 h. The ratio of the reporter protein to ACTB band density was statistically calculated by ImageJ. The error bar represents the mean \pm SD of the three biological replicates. ANOVA was used to analyze multiple sets of data. Different letters indicate statistically significant differences ($p < 0.05$). $n = 3$ for all graphs and see Additional file 2

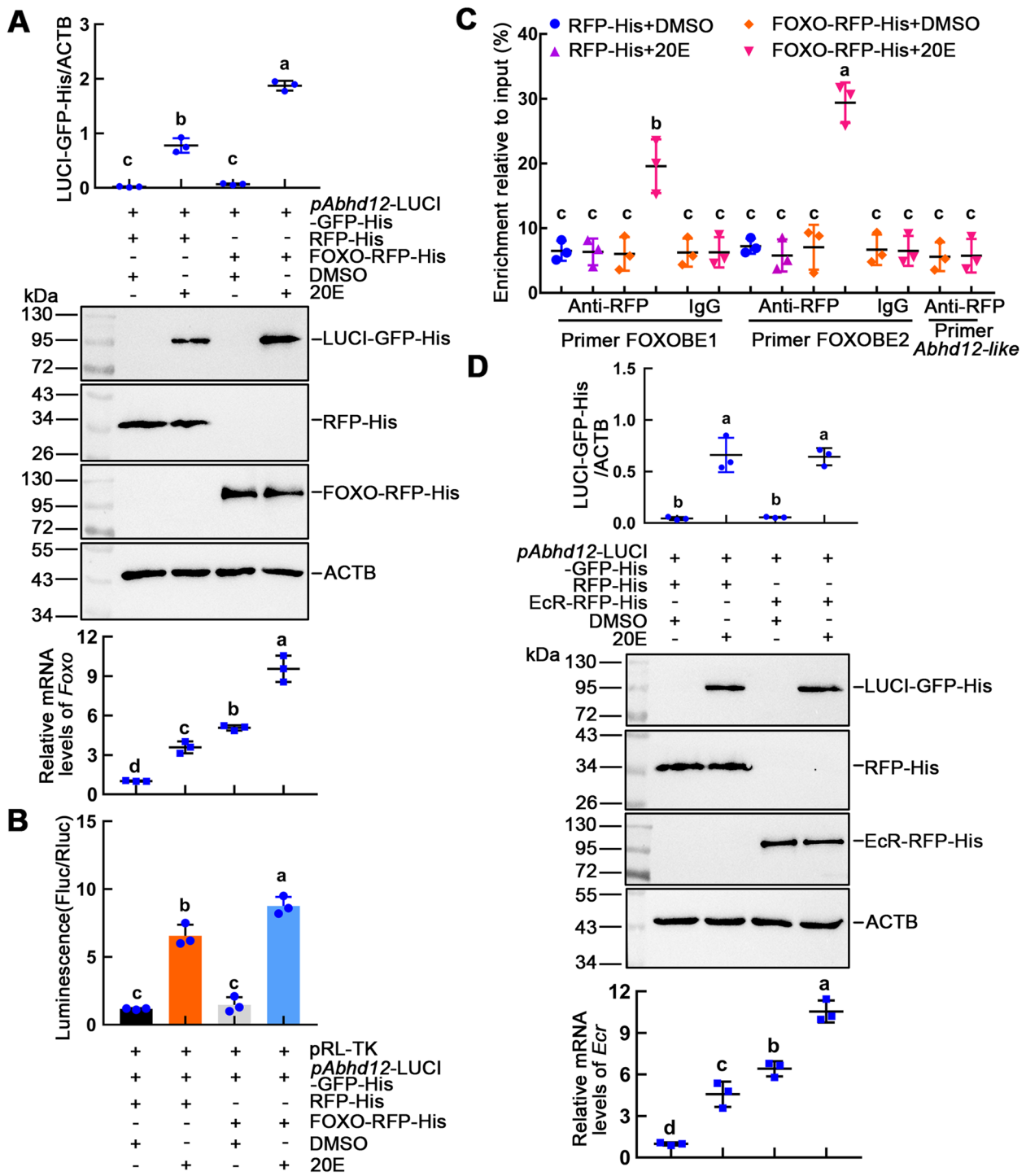


Fig. 5 (See legend on previous page.)

after knockdown of *Abhd12-like* (Fig. 7E and F). The larvae showed delayed pupation after injecting *dsAbhd12-like* (Fig. 7G); all the larvae's average pupation time was delayed by 11 h compared with that in larvae injected with *dsGfp*, and 33% of the larvae had delayed pupation

time of approximately 24 h compared to the control group's average pupation time (Fig. 7H and I). When *dsAbhd12-like*-treated, the average weight of pupae did not significantly change, compared with larvae injected with *dsGfp* (Fig. 7J). In addition, the *dsAbhd12-like*

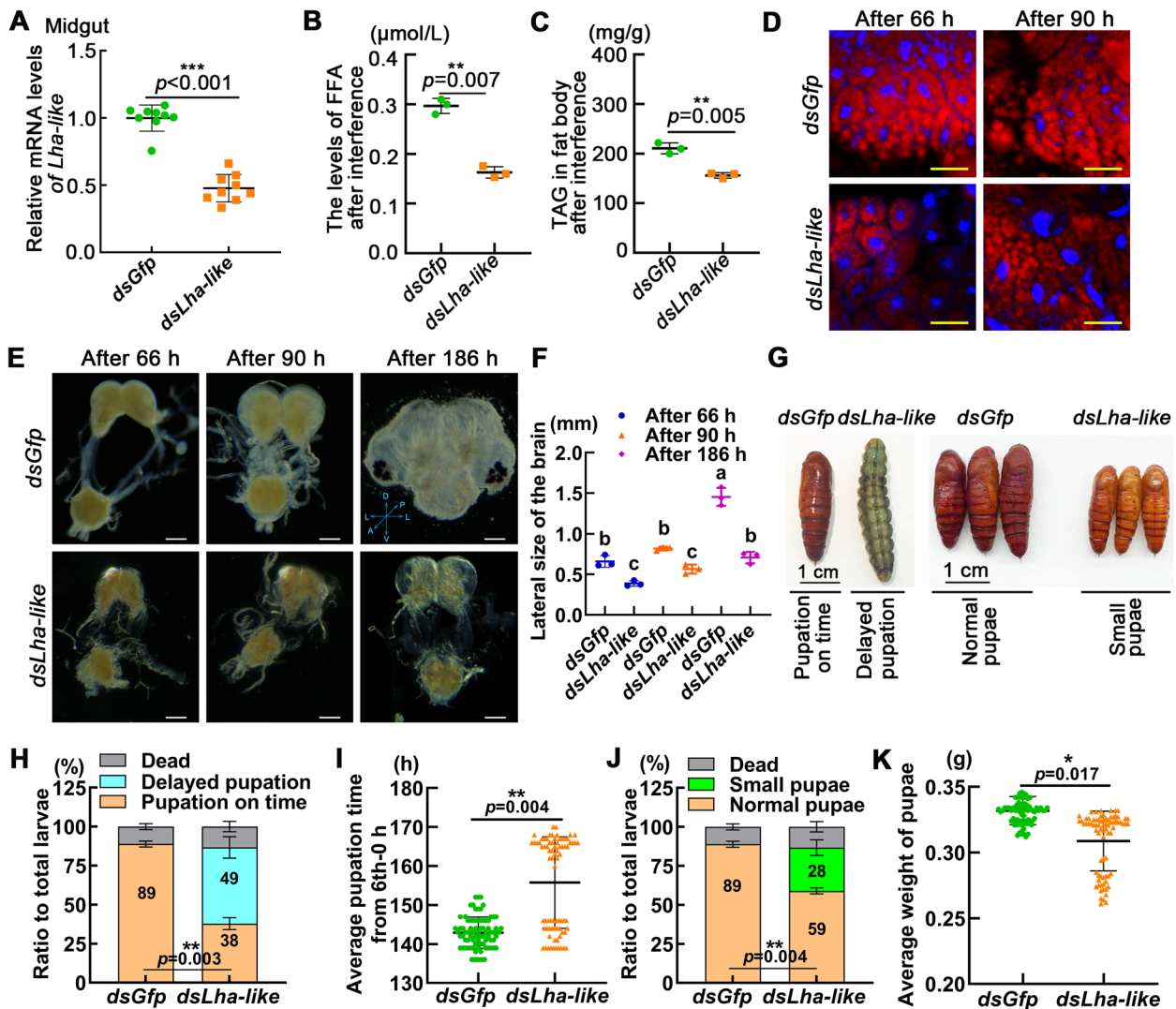


Fig. 6 Knockdown of *Lha-like* delayed pupation and decreased pupae weight. **A** The interference efficiency in the midgut after the fourth dsRNA injection. $n = 9$. **B** FFA levels in the hemolymph after the fourth dsRNA injection 24 h. $n = 3$. **C** The TAG levels in the fat body after fourth dsRNA injection 24 h. $n = 3$. **D** Nile red staining showing LDs after knockdown of *Lha-like*, observed for 66 h and 90 h after the first dsRNA injection. The scale bar represents 50 μm . **E** The brain morphology, after knockdown of *Lha-like*, was observed for 66 h, 90 h, and 186 h after the first injection of dsRNA. The bars represent 200 μm . Back view. Directions: A, anterior; D, dorsal; L, lateral; P, posterior; V, ventral. **F** Quantification of the data in (E). $n = 3$. **G** Phenotypes after *Lha-like* knockdown (2 $\mu\text{g}/\text{larva}$ at fifth instar 20 h, four times at a 24 h interval). Scale bar: 1 cm. The phenotype images of pupation on time and normal pupae exhibit 2-day-old pupae. The phenotype image of delayed pupation exhibits sixth instar 166 h larva. The phenotype image of small pupae exhibits 1-day-old pupae. **H** Ratio of phenotypes of delayed pupation. $n = 30 \times 3$ (three replicates, 30 larvae each). **I** Statistics of pupation time from sixth instar 0 h to pupae. The time point of the fifth instar larvae transforming into the sixth instar larvae after molting, representing the sixth instar 0 h (6th-0 h). 6th-0 h larvae indicate that larvae have just entered the sixth instar stage. In the *dsGfp* group, n for each experiment was 27, 26, and 27 respectively; in the *dsLha-like* group, n for each experiment was 25, 26, and 27 respectively. **J** The percentage of small pupae. $n = 30 \times 3$. **K** Statistics of average pupae weight in the *dsLha-like* and *dsGfp* groups. In the *dsGfp* group, n for each experiment was 27, 26, and 27 respectively; in the *dsLha-like* group, n for each experiment was 25, 26, and 27 respectively. The error bar represents the mean \pm SD of the three biological replicates, and Student's t test analysis indicated significant differences ($*p < 0.05$, $**p < 0.01$, and $***p < 0.001$). Multiple sets of data were compared by analysis of variance (ANOVA), and different letters represent significant differences ($p < 0.05$). n indicates the number of data points and Additional file 2 for individual data values

injection caused the midgut to appear red later than the *dsGfp* group (Additional file 1: Fig. S8D). HE staining showed that the larval midgut (LM) separated from

the imaginal midgut (IM) in the *dsAbhd12-like*-treated larval later than the larvae injected with the *dsGfp* (Additional file 1: Fig. S8E). Similarly, after injection of

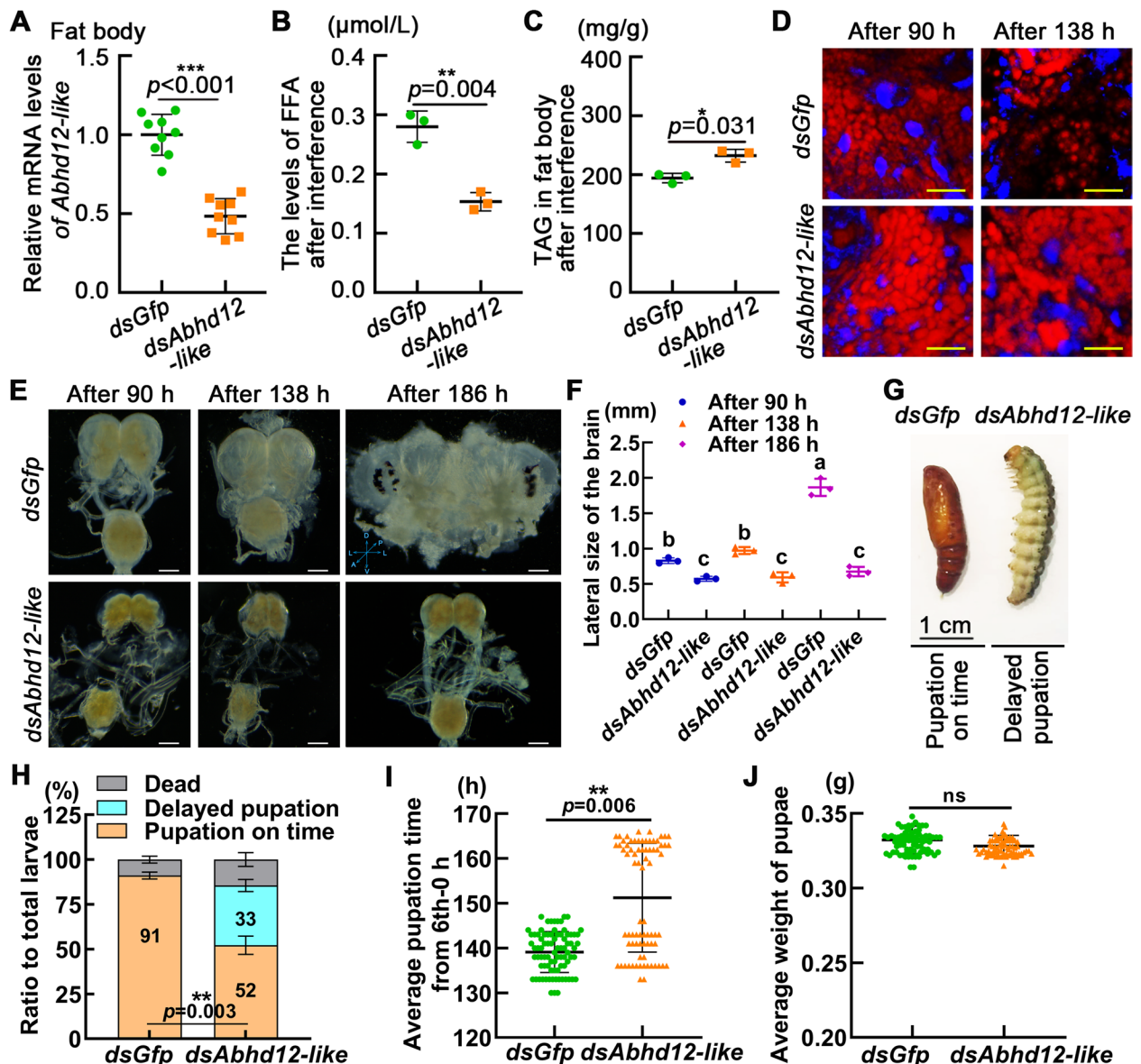


Fig. 7 Injection of *dsAbhd12-like* led to delayed pupation. **A** The interference efficiency of *Abhd12-like* in the fat body after the fourth dsRNA injection. $n = 9$. **B** FFA levels in the hemolymph after the fourth dsRNA injection 24 h. $n = 3$. **C** The TAG levels in the fat body after the fourth dsRNA injection 24 h. $n = 3$. **D** Nile red staining showing LDs after *Abhd12-like* knockdown, observed 90 h and 138 h after the first dsRNA injection. The scale bar represents 50 μm . **E** Brain morphology observed after the knockdown of *Abhd12-like* and the first injection of dsRNA for 90 h, 138 h, and 186 h. The scale bars represent 200 μm . Back view. Directions: A, anterior; D, dorsal; L, lateral; P, posterior; V, ventral. **F** Quantification of the data in (E). $n = 3$. **G** Phenotypes after *Abhd12-like* knockdown (2 $\mu\text{g/larva}$ at sixth instar 6 h, four times at a 24 h interval). Scale bar: 1 cm. The phenotype image of pupation on time exhibits 2-day-old pupae. The phenotype image of delayed pupation exhibits sixth instar 163 h larva. **H** Ratio of phenotypes of pupation on time exhibits 2-day-old pupae. The phenotype image of delayed pupation exhibits sixth instar 163 h larva. **H** Ratio of phenotypes of pupation on time exhibits 2-day-old pupae. $n = 30 \times 3$ (three replicates, 30 larvae each). **I** Statistics of pupation time from 6th-0 h to pupae. In the *dsGfp* group, n for each experiment was 27, 27, and 28 respectively; in the *dsAbhd12-like* group, n for each experiment was 25, 25, and 27 respectively. **J** Statistics of average pupae weight in the *dsAbhd12-like* and *dsGfp* groups. In the *dsGfp* group, n for each experiment was 27, 27, and 28 respectively; in the *dsAbhd12-like* group, n for each experiment was 25, 25, and 27 respectively. Statistical analysis was conducted using Student's *t* test ($*p < 0.05$, $**p < 0.01$, and $***p < 0.001$) or ANOVA, and different letters represent significant differences ($p < 0.05$). The error bar represents the mean \pm SD of the three biological replicates. n indicates the number of data points and Additional file 2 for individual data values

dsAbhd12-like, the morphology and HE staining of the fat body also demonstrated that the degradation of the fat body was delayed, too (Additional file 1: Fig. S8F and

G). The expression of *Lip3-like*, *Ptl-like X2*, and *Plrp2* was detected to show that there was no off-target effect of *Abhd12-like* knockdown (Additional file 1: Fig. S8H).

These results suggested that ABHD12-like degrades TAGs in the fat body to release FFAs and support the development of adult tissue, including the brain.

Discussion

FFAs are essential for animal development as energy sources and cell structure components. This study revealed that lipases play important roles in maintaining FFA homeostasis during feeding and nonfeeding stages. JH III and 20E upregulate the expression of different lipases through different transcription factors to maintain the dynamic balance of FFAs in hemolymph and ensure the energy and material supply for insect development.

Lipases play important roles in maintaining FFA homeostasis for development during larval feeding and metamorphosis

Lipid metabolism is the core process of energy homeostasis regulation. Dietary TAGs are broken down by the main dietary lipases GL and PTL to release FAs. The midgut of insects is mainly responsible for the digestion and absorption of lipids, which can be digested by lipase to produce FFAs, glycerol, and other compounds. Dietary fat hydrolysis produces FFAs, which can provide energy through β -oxidation for body growth [37], and FFAs can also be re-esterified to form lipids for energy storage [38, 39]. These FAs are absorbed by the intestine and used to resynthesize TAGs that migrate to the adipose tissue for storage [40–42]. In this study, we identified the dietary lipase LHA-like, which is closely related to the human PTL family, as a critical lipase that decomposes dietary TAGs in the midgut during the feeding stage. Therefore, LHA-like is an essential lipase that maintains the homeostasis of FFAs in the hemolymph and energy storage in the fat body during feeding condition to ensure larvae growth, development, and metamorphosis.

Insects need nutrients from their diet. The gut is its central organ for digesting food and absorbing nutrients. Intestinal cells in the midgut are responsible for producing digestive enzymes and absorbing digestive products [43]. Insects rely on the hydrolysis of digestive enzymes to digest proteins, carbohydrates, and lipids in food, and the food is processed in the gut; the end products of digestion are absorbed by the midgut epithelial cells. The absorbed molecules can then be further processed within the epithelium or released from the basal membrane into the hemolymph, transported to their respective sites of action or specific storage tissues [5]. We found that LHA-like, as a gut-digestive enzyme, can hydrolyze dietary lipids and the lipids are absorbed through the gut–hemolymph barrier to support the development of a variety of tissues and individuals.

During nutrient deprivation, the stored TAG of the body can be accessed to release FAs through the action of specific lipases for energy production through mitochondrial fatty acid β -oxidation. Defects in these processes can lead to dramatic changes in TAG and FFA levels and the development of various diseases, including obesity, diabetes, and cardiovascular disease [44, 45]. During the period of high energy demand or starvation, insects use lipid hydrolysis in the fat body to produce FFAs for β -oxidation or use FFAs and other substrates to provide energy through gluconeogenesis as needed by the body [32, 46]. Our study found that ABHD12-like produces FFA during nonfeeding stages in metamorphosis by hydrolyzing stored TAG in the fat body. The FFA levels are higher in the feeding stage than in the metamorphic stage, because FFAs are used for gluconeogenesis to produce glucose [32]. ABHD12-like is an important lipase that maintains FFA homeostasis to ensure energy supply for adult tissue development by hydrolyzing TAG in the fat body at nonfeeding stages during metamorphosis.

Glucose is the most important substrate for the energy supply in the brain [47]. *Drosophila* glial cells with impaired glycolysis rely on mitochondrial fatty acid breakdown to maintain adequate neuronal nutrient supply [30]. FAs enter the human brain via carrier-mediated transport, including fatty acid transport proteins (FATP), fatty acid binding protein 5 (FABP-5), and fatty acid translocase/CD36 [48]. There are few studies on the mechanism of FA uptake in the central nervous system of insects compared with vertebrates. *Drosophila* has one FABP ortholog, dFabp; knocking down *dFabp* in neurons results in increased apoptosis in the brain [49]. *Drosophila* FATP shows high homology to human and mouse FATP1 and FATP4, and *fatp* mutants are lethal in *Drosophila* [50, 51]. This study found that peripheral lipases LHA-like and ABHD12-like hydrolyze TAG to maintain FFA homeostasis, which is very important for brain development. One mechanism of FFA homeostasis promoting brain development is that FFAs may supply energy for brain development through β -oxidation or gluconeogenesis pathway.

There are many circulating lipids that affect development, such as FFAs, DAGs, etc. [52–54]. In this study, we revealed the effect of FFA homeostasis on the metamorphosis and development of *H. armigera*. The FFAs produced by lipid hydrolysis may be transported into the circulatory system or tissues to affect the development of the tissues. In starvation, FFAs are raw energy materials for most tissues, and glial cells in the brain can also use FFAs to obtain energy [30]. In addition, glucose is the preferred energy source for tissue energy supply. During metamorphosis, insects stop feeding and can produce glucose through gluconeogenesis. FFAs are substrates

of gluconeogenesis [32]. The effects of other circulating lipids on tissue and individual growth need to be further elucidated.

Lipases are differentially regulated by different hormones

In humans, insulin inhibits the decomposition of TAGs and promotes the accumulation and storage of TAGs in adipocytes [55]. In the present study, we found that JH III increased the transcription of *Lha-like* via its intracellular receptor MET. MET exists in the form of the homologous dimer, which needs to be separated by JH treatment, then MET forms a heterodimer with TAI to combine with JHRE to promote gene transcription [56, 57]. In *H. armigera*, the phosphorylated MET and TAI form a complex under JH regulation, which binds to JHRE to promote Krüppel homolog (Kr-h1) transcription [58]. In addition to JH regulation, we found that insulin can also induce the expression of *Lha-like*. The basal expression of the reporter without JH III induction might be the result of the insulin signal and the endogenous MET1 in the cells. Therefore, *Lha-like* is regulated by both JH and insulin, which is consistent with the characteristic that the dominant hormones at the feeding stage are insulin [24] and JH [59]. Insulin and JH exert synergistic effects and cooperate to regulate insect growth [60, 61]. The expression of *Lha-like* is not upregulated by 20E, which is consistent with the low 20E titer during insect feeding [62]. In addition to *Lha-like*, we found that *Ptl-like*, *Plrp2-like*, and *Liph-like* were also highly expressed during the feeding stage, and JH upregulate their expression. PTL-like, PLRP2-like, and LIPH-like belong to the pancreatic lipase superfamily, and it is speculated that they play a role in hydrolyzing dietary TAG during the feeding period. However, which transcription factors directly regulate their expression under JH treatment and whether other hormones are involved in regulating their expression still need to be further explored. The results of this study reveal the mechanism of FFA production and hormonal regulation of the related lipases during the feeding stage in insects.

Steroid hormones regulate lipid metabolism in the opposite way of insulin. For example, adrenaline can activate lipases, thus accelerating the hydrolysis of TAGs in mouse adipocytes [63]. Glucocorticoids also play a role in promoting lipolysis by increasing the transcription and expression of lipases [64]. 20E, a steroid hormone, is the master hormone during insect metamorphosis. 20E regulates gene expression via G protein-coupled receptors and the nuclear receptor EcR [26]. In murine adipocytes, FOXO1 induces ATGL expression, thus promoting lipolysis [65]. In insects, *Drosophila* FOXO mutation reduces the expression level of *Brummer* in the fat body [66]. The acid lipase

gene *Dlip4* is upregulated by FOXO in *Drosophila* [67]. In *B. mori*, 20E upregulates the expression of *Brummer* enzyme and *acid lipase-1* by activating FOXO transcriptional activity and promoting lipolysis of the fat body during the molting and pupation stages [68]. Here, we found a monoacylglycerol lipase *Abhd12-like* that is highly expressed in the metamorphic phase and is upregulated by 20E via FOXO and EcR. However, EcR does not directly regulate *Abhd12-like* expression but instead upregulates FOXO expression, which in turn upregulates *Abhd12-like* expression. The activity of FOXO is affected by various post-translational modifications, such as acetylation, phosphorylation, and ubiquitination. The cells respond to different environments; FOXO with different post-translational modifications, altering transcriptional activity, subcellular localization, or interacting with other proteins [69]. In mammals, histone acetyltransferase CREB-binding protein (CBP) catalyzes the acetylation of FOXO [70]. Different acetylation sites of FOXO are associated with its nuclear translocation and transcriptional activity [71–73]. In *H. armigera*, 20E promotes gene transcription by inducing FOXO acetylation through histone acetyltransferase 8 (KAT8) [74]. We found that overexpression of FOXO under 20E treatment activates *Abhd12-like* transcription, implying that post-translational modification of 20E-regulated FOXO is necessary for its activation of *Abhd12-like*.

The holometabolous insect transition from the final instar larva to adult is called metamorphosis. During metamorphosis, the larva stops feeding, begins to wander, and finally becomes stationary before pupating. Insulin and 20E are significant regulators of insect growth [75]. JH, Insulin promotes growth and ecdysone production in the prothoracic gland (PG), followed by elevated 20E levels that inhibit insulin function and promote insect metamorphosis [76]. High titer 20E counteracts the insulin pathway by dephosphorylating insulin receptor (INSR), thereby preventing larva growth and accumulation of glucose in hemolymph [24]. Starvation and 20E-induced stop-feeding during metamorphosis are different states. 20E actively initiates signal transduction, such as dopamine (DA) binds to the dopamine receptor (DopEcR) to promote feeding and growth of larvae, while 20E competes with DA to bind DopEcR to inhibit feeding and promote metamorphosis [62]. 20E and starvation treatment can induce the similar effects, such as autophagy and apoptosis [77, 78], but some effects are different, such as long-term starvation of larvae leads to the prolongation of the feeding period [79], while 20E treatment leads to the early occurrence of premature metamorphosis [80]. We found that *Abhd12-like* expression is not affected by insulin and JH III, which is

consistent with the high 20E titer during metamorphosis [62].

Conclusions

During the feeding stage, JH upregulated the expression of *Lha-like* in the midgut via MET1, degrading dietary TAG to produce FFAs for larval growth and TAG storage. During the metamorphic stage, 20E upregulated the expression of *Abhd12-like* via FOXO, degrading TAGs stored in the fat body to produce FFAs for metamorphosis. JH and 20E maintain the homeostasis of FFAs at the feeding and metamorphic stages by upregulating the expression of different lipases via different transcription factors. The homeostasis of FFAs during the feeding and nonfeeding stages ensures larval growth, brain development, and metamorphosis (Fig. 8).

Methods

Experimental animals

H. armigera (cotton bollworms) were reared on an artificial diet in our laboratory at $27 \pm 1^\circ\text{C}$ with 40–70% relative humidity under a light:dark schedule of 14 h:10 h. The artificial feed was composed of soybean powder, wheat g powder, multivitamins, sucrose, and inorganic salts to feed larvae [81].

Experimental cells

The *H. armigera* epidermal cell line (HaEpi) was established and maintained in our laboratory [34] at 27°C in Grace's insect cell culture medium (Gibco, USA, California) supplemented with 10% fetal bovine serum (Biological Industries, Cromwell, CT, USA).

Bioinformatics analysis

First, we used "lipase" as a key word to search the genome database of *H. armigera*, and then a total of 107 genes containing lipase words in their annotated names were found. In general, lipase proteins have a conserved motif of sequence Gly-X-Ser-X-Gly (GX SXG) and a typical α/β -hydrolase domain [82]. ATGL with a patatin domain [83]. In *B. mori*, some lipases without conserved GX SXG motifs [84]. We further used the amino acid sequences of lipases from *B. mori*, *D. melanogaster*, and *H. sapiens* for BLAST analysis in the *H. armigera* genome database. Finally, 97 proteins encoded by 83 genes were identified as belonging to the lipase family. The analysis of 97 proteins using phylogenetic tree and domain prediction showed that all of them were lipases. The full length of the protein sequence was obtained from NCBI (<https://www.ncbi.nlm.nih.gov/>), and MEGA7.0 was used for phylogenetic tree analysis. The structural domains of the obtained proteins were predicted using SMART (<http://smart.embl-heidelberg.de/>). The heatmap was obtained

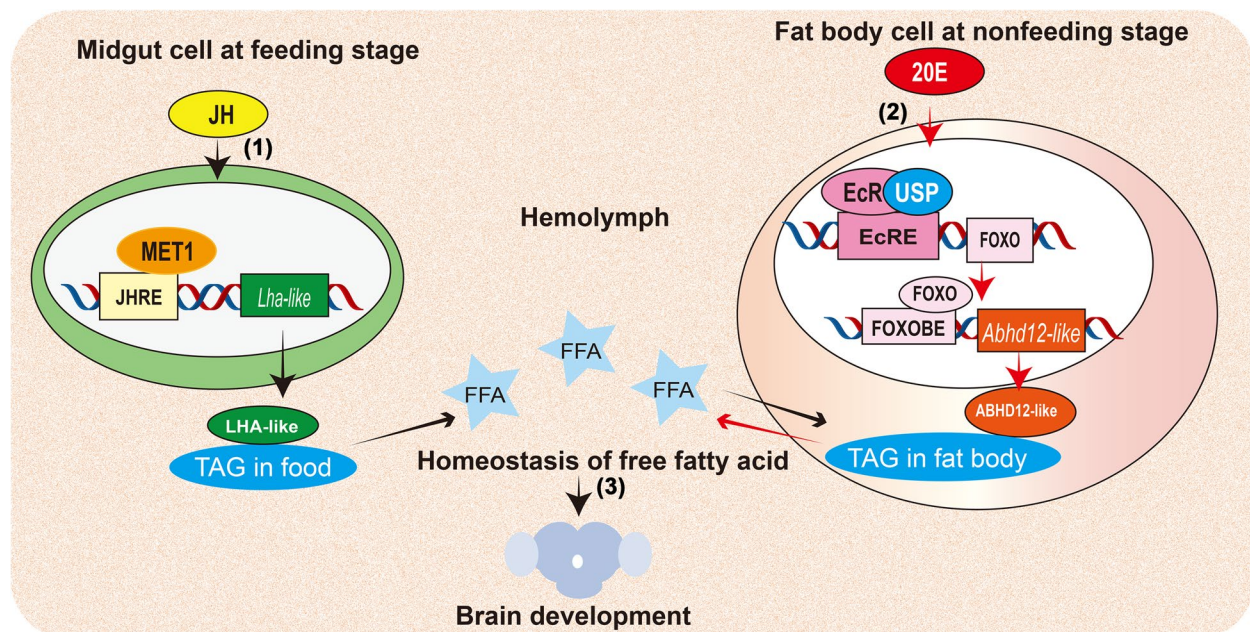


Fig. 8 A diagram illustrating that JH and 20E regulate FFA homeostasis. JH upregulates the transcription of *Lha-like* via the intracellular receptor MET1. LHA-like contains signaling peptides, which are secreted to midgut to hydrolyze dietary TAG to produce hemolymph FFAs and fat body TAG (1). Whereas, 20E upregulates the expression of *Abhd12-like* via FOXO. ABHD12-like promotes the hydrolysis of fat body TAG to compensate the FFAs in hemolymph during metamorphosis (2), thus maintaining FFA homeostasis in larval hemolymph at the feeding and metamorphic stages for brain development (3)

from the website (<https://www.omicstudio.cn/tool>). The transcription factor binding motifs were predicted by the JASPAR transcription factor database (<http://jaspar.genereg.net/>).

JH III and 20E induction in larvae

JH III and 20E powder were dissolved in dimethyl sulfoxide (DMSO), and the stock solution was 20 mM. The stock solution was diluted in phosphate-buffered saline (PBS, 140 mM NaCl, 10 mM sodium phosphate, pH 7.4) when needed. JH III or 20E was injected into the sixth instar 6 h larval hemocoel. An equal amount of diluted DMSO was used as a control.

Quantitative real-time reverse transcription PCR (qRT-PCR)

Total RNA was extracted with TRIzol reagent according to the manufacturer's instructions (TransGen Biotech, Beijing, China), and then the RNA concentration was determined. RNA (2 µg) was reverse-transcribed into first-strand cDNA using a cDNA synthesis kit (Abm, Richmond, Canada). qRT-PCR was performed with a qTOWER³/G system (Analytik Jena AG, Jena, Germany) with a reaction mixture (10 µL) containing 5 µL of TransStart Tip Green qPCR Supermix (Aidlab, Beijing, China), 1 µL of cDNA, and 2 µL each of the forward and reverse primers (1 µM) (sequences shown in Additional file 1: Table S1). The *H. armigera* β -actin gene (*Actb*) was used as an internal reference. Data were analyzed by the formula $R = 2^{-\Delta\Delta CT}$ method ($\Delta\Delta CT = \Delta CT_{\text{sample}} - \Delta CT_{\text{control}}$, $\Delta CT = CT_{\text{gene}} - CT_{\text{actin}}$) [85].

Synthesis of double-stranded RNA (dsRNA)

The long dsRNA sequence was broken down into smaller fragments in vivo, specifically inhibiting the expression of the target genes in worms [86, 87]. RNA interference (RNAi) efficiency has been tested in a variety of moths [88]. RNAi primers containing the T7 sequence (Additional file 1: Table S1) were used to obtain the DNA template by PCR. The DNA template (2 µg), 5× transcription buffer (20 µL), T7 RNA polymerase (3 µL, 20 U/µL), A/U/C/GTP (2.4 µL, 10 mM), RNase inhibitor (3 µL, 40 U/µL, Thermo Fisher Scientific, Waltham, USA), and RNase-free water were mixed, and the final volume was 50 µL. After incubation at 37°C for 4–6 h, 10 µL of RNase-free DNase I (1 U/µL, Thermo Fisher Scientific), 10 µL of DNase I Buffer, and 30 µL of RNase-free water were added to the solution, which was incubated at 37°C for 1 h. The product was purified with phenol/chloroform and precipitated with ethanol and 3 M sodium acetate (prepared with DEPC water, pH 4.5); the sediment was dissolved in 30 µL of RNase-free water. The purity and integrity of the dsRNA were determined using agarose gel electrophoresis. The concentration of dsRNA was

measured by a MicroSpectrophotometer (GeneQuant; Amersham Biosciences, Little Chalfont, UK).

RNA interference

Sterile 1×PBS was used to dilute dsRNA to 400 ng/µL. The fifth instar 20 h or sixth instar 6 h larvae were randomly selected, and then larvae were placed on ice for 30 min and injected with 2 µg dsRNA into the larval hemocoel by a microsyringe. The larvae were injected at an interval of 24 h for a total of four times. RNA was extracted 12 or 24 h after the fourth injection and reverse-transcribed into cDNA for qRT-PCR experiments. *Met1*, *Foxo*, and *Ecr* were interfered, 500 ng of JH III or 20E was injected 12 h after the third injection, and the same volume of DMSO was used as the control.

Construction of the LUCI-GFP-His plasmid

The full-length cDNA sequence of luciferase was cloned, with a total of 1650 bp. The recombinant plasmid pIEx-4-luciferase-GFP-His was constructed by inserting it into the polyclonal site between Sac I and Pst I of pIEx-4-GFP-His. The IE promoter and hr5 enhancer (1112 bp in total) of the recombinant pIEx-4-luciferase-GFP-His plasmid were cleaved with Sma I and Sac I, and replaced with the 5' upstream sequence of *Lha-like* (-1292~ATG) or the 5' upstream sequence of *Abhd12-like* (-2142~ATG) to construct the reporter gene plasmid.

Dual-luciferase reporter assay

After the confluence of HaEpi cells reached 70–80% in six-well plates, the reporter plasmid, pRL-TK, and MET1-RFP-His or FOXO-RFP-His were cotransfected into HaEpi cells. RFP-His was overexpressed as a negative control. The reporter plasmid containing target promoter driving firefly luciferase (Fluc), the reference pRL-TK plasmid (Promega, E2241) containing HSV-TK promoter driving renilla-luciferase (Rluc). The promoter of the HSV-TK in pRL-TK plasmid drives the expression of the renilla luciferase in insect cells [89]. After 48 h of cotransfection, 2 µM JH III or 2 µM 20E was added for 24 h, and the same volume of DMSO was used as the negative control. The cells were washed three times with PBS. The lysis buffer was diluted with sterile water at 4:1, and then the lysis buffer was incubated with the cells on a microvibrator at room temperature. The lysis products were centrifuged at 12,000×g for 5 min, and the supernatant was collected. D-luciferin was dissolved with firefly luciferase assay buffer to prepare a 0.2 mg/mL firefly luciferase detection solution. 50×coelenterazine renilla luciferase assay buffer was diluted to a 1×coelenterazine working solution. Luciferase activity was measured using the Dualucif Firefly and Renilla Assay Kit (UElandy, Suzhou, China) according to the instructions. A multimode plate

reader was used to measure the values (EnSpire, PerkinElmer, Waltham, USA).

Western blotting

Total proteins were extracted from cells. Total proteins (20 μ g) from each sample were subjected to 10% sodium dodecyl sulfate–polyacrylamide gel electrophoresis (SDS–PAGE) and then electrophoretically transferred onto a nitrocellulose membrane. The membrane was incubated with blocking solution containing 3% skim milk in Tris-buffered saline (TBST, 10 mM Tris–HCl and 150 mM NaCl, pH 7.5, 0.02% tween) for 1 h at room temperature. The primary antibodies were added to fresh blocking buffer and incubated overnight at 4°C. The primary antibodies, including RFP, GFP, and ACTB (ABclonal, Wuhan, China), were diluted at 1:5000. After being washed two times with TBST for 10 min each time and then washed one time for 10 min with TBS, the membrane was incubated with diluted secondary antibodies (ZSGB-BIO, Beijing, China) labeled with horseradish peroxidase (1:7000 in blocking buffer) for 2 h at room temperature. The membrane was washed two times for 10 min each with TBST and then washed once for 10 min with TBS. The membrane was incubated with High-sig ECL Western Blotting Substrate (Tanon Science & Technology, Shanghai, China). The immunoreactive protein bands were detected by a chemiluminescence imaging system (Tanon Science & Technology).

Chromatin immunoprecipitation (ChIP) assay

The 5 μ g MET1-RFP-His, FOXO-RFP-His, or RFP-His plasmid was transfected into cells for 72 h. The cells were then treated with JH III (2 μ M) or 20E (2 μ M) for 6 h. DMSO treatment was used as a control. The ChIP Assay Kit (Beyotime Biotechnology, Shanghai, China) was used according to the instructions. The cells were then incubated with 1% formaldehyde and crosslinked at 37°C for 10 min. The crosslinking was terminated by adding glycine (0.125 M) for 10 min. After washing the cells with PBS for three times, SDS lysis buffer (1% SDS, 10 mM EDTA, 50 mM Tris–HCl, pH 8.1) was added to re-suspend the cells. DNA was cleaved into fragments of 200 to 1000 bp using a Bioruptor Pico (Diagenode). The samples were centrifuged to collect the supernatant at 4°C for 15 min, and then 50 μ L of protein A/G resin was added and incubated at 4°C for 1 h to exclude nonspecific binding. After centrifugation, 50 μ L supernatant sample was used as an input sample for qRT-PCR. Other supernatant samples were incubated with anti-RFP antibody or mouse control IgG as a negative control at 4°C overnight. Then, 50 μ L of protein A/G resin was mixed with the immunoprecipitated protein–DNA complex and incubated at 4°C for 2 h. The complexes of protein–DNA–resin were

washed once with low-salt wash buffer (0.1% SDS, 1.0% Triton X-100, 2 mM EDTA, 200 mM Tris–HCl, pH 8.0, 150 mM NaCl), followed by washing with a high-salt wash buffer (0.1% SDS, 1.0% Triton X-100, 2 mM EDTA, 20 mM Tris–HCl, pH 8.0, 500 mM NaCl), LiCl wash buffer (10 mM Tris–HCl, pH 8.1, 0.25 M LiCl, 1 mM EDTA, 1% NP-40, 1% deoxycholate), and twice with TE buffer (10 mM Tris–HCl, pH 8.1, 1 mM EDTA). The protein–DNA–resin complexes were then washed with elution buffer (1% SDS, 0.1 M NaHCO₃). The complexes were reverse cross-linked at 65°C overnight, followed by RNase A and proteinase K treatments. The DNA was purified using phenol/chloroform extraction and analyzed by qRT-PCR with target primers (Additional file 1: Table S1).

Free fatty acid (FFA) level determination

Fifty microliters of hemolymph from the corresponding sample larvae were mixed with phenylthiourea (PTU) to prevent hemolymph melanization, and the reagents were added according to the FFA kit instructions (Solarbio, Shanghai, China). The absorbance was measured at a wavelength of 550 nm using spectrophotometry. The standard curve was created by diluting the standard to various concentrations. The concentration of the standard solution is the x -axis, and $\Delta A^{\text{standard}}$ ($\Delta A = A^{\text{standard tube}} - A^{\text{blank tube}}$) is the y -axis, and the equation $y = kx + b$ is obtained, and the FFA levels were estimated using the standard curve.

Triglyceride (TAG) level determination

The reagents were preequilibrated to room temperature. A 1 mg/mL standard solution was prepared. A total of 0.1 g of fat body was taken for analysis according to the instructions of the TAG detection kit (Solarbio, Beijing, China). The absorbance value was measured by spectrophotometry at 420 nm (Infinite M200PRO NanoQuant, Tecan, Switzerland).

Nile red staining

The frozen sections were dried at room temperature. The tissues were fixed in 4% paraformaldehyde solution at room temperature for 30 min. The sections were washed with PBS. Fifty microliters of proteinase K solution (20 μ g/mL) were added to each sample and incubated for 20 min at room temperature. The sections were washed with PBS. The tissue was incubated with Nile red (MCE, New Jersey, UAS) solution at 37 °C for 30 min in the dark. The dye solution was removed, and the cells were washed with PBS in the dark. DAPI (BBI LIFE SCIENCE, Shanghai, China) solution was incubated in the dark for 10 min. The dye solution was removed, and the cells were rinsed in the dark with PBS. The anti-fluorescence quencher

was added to tissue slides, and the slides were sealed for observation.

Statistical analysis

The protein bands obtained by western blotting were quantified by ImageJ software. GraphPad Prism 9 (GraphPad Inc., La Jolla, CA, USA) was used to analyze the data, and the resulting diagram is shown. According to three biological repetitions, the differences between the two groups of data were analyzed by a two-tailed Student's *t* test. Asterisks in the figure indicate significant differences among groups ($^*p < 0.05$ means significant differences, $^{**}p < 0.01$ and $^{***}p < 0.001$ means extremely significant differences). Analysis of variance (ANOVA) was used for multiple group comparisons. The different lowercase letters show the significant differences. Bars are shown as means \pm SD.

The antibodies used in this study

The monoclonal anti-GFP antibody (Cat. AE012, RRID: AB_2770402), monoclonal anti-RFP antibody (AE020, RRID: AB_2770409), and polyclonal anti-ACTB antibody (Cat. AC026, RRID: AB_2768234) were obtained from ABclonal Technology (ABclonal, Wuhan, China).

Abbreviations

20E	20-Hydroxyecdysone
JH	Juvenile hormone
TAG	Triglyceride
FFA	Free fatty acid
PTL	Pancreatic lipase
LHA-like	Lipase member H-A-like
ABHD12-like	α/β -Hydrolase domain-containing protein 12
MGL	Monoacylglycerol lipase
MET1	Methoprene-tolerant 1
FOXO	Forkhead box O
LL	Lingual lipase
GL	Gastric lipase
PLRP	Pancreatic lipase-related proteins 1, 2, and 3
LPL	Lipoprotein lipase
HL	Hepatic lipase
ATGL	Adipose triglyceride lipase
HSL	Hormone-sensitive lipase
DAG	Diacylglycerol
MAG	Monoacylglycerol
GC	Glucocorticoid
GR	Glucocorticoid receptor
GH	Growth hormone
STAT5	Signal transducer and activator of transcription 5
ACTH	Adrenocorticotrophic hormone
SF-1	Steroidogenic factor-1

Supplementary Information

The online version contains supplementary material available at <https://doi.org/10.1186/s12915-024-01973-3>.

Additional file 1: Figs S1–S8, Table S1. Fig. S1 The structural domain analysis of LIPASE in *H. armigera*. Fig. S2 Different expression levels of lipases in *H. armigera* by transcriptomics. Fig. S3 The expression profiles and hormone induction of lipases in vivo. Fig. S4 The hormone regulation of *Lha-like* and *Abhd12-like*. Fig. S5 Construction of pIEx-4-LUCI-GFP-His vector. Fig. S6

The map of *pAbhd12-LUCI-GFP-His* reporter plasmid. Fig. S7 Knockdown of *Lha-like* resulted in delayed development in the midgut and fat body. Fig. S8 Knockdown of *Abhd12-like* delayed metamorphosis and tissue remodeling. Table S1. Oligonucleotide sequences of PCR primers.

Additional file 2: The individual data values for Fig. 2A–F, Fig. 3B, D–F, Fig. 4B, D, Fig. 5A–D, Fig. 6A–C, F, H–K, Fig. 7A–C, F, H–J, Fig. S2A–C, Fig. S3A–I, Fig. S4A–D, Fig. S7B, C, H, and Fig. S8B, C, H.

Additional file 3: Original Western blot data

Acknowledgements

We thank Xiangmei Ren at the State Key Laboratory of Microbial Technology, Shandong University, for helping us use the plate reader. We thank Jingyao Qu, Zhifeng Li, and Jing Zhu at the State Key Laboratory of Microbial Technology, Shandong University for help helping us use the cell crusher.

Authors' contributions

Y.L., Q.Y., and X.Z. conceived and designed the research. Y.L., Q.Y., and T.L. performed the experiments and analyzed the data. Y.L., Q.Y., J.W., and X.Z. contributed to the experiment design and manuscript preparation. Y.L., Q.Y., and X.Z. wrote the manuscript. All authors read and approved the final manuscript.

Funding

This work was supported by the National Natural Science Foundation of China (Grant nos. 32330011 and 32270507).

Availability of data and materials

All data generated or analyzed during this study are included in this published article and its supplementary information files. The individual data values of all experiments are presented in Additional file 2.

Declarations

Ethics approval and consent to participate

Not applicable.

Consent for publication

Not applicable.

Competing interests

The authors declare no competing interests.

Received: 28 January 2024 Accepted: 5 August 2024

Published online: 13 August 2024

References

- Martin-Perez M, Urdiroz-Urricelqui U, Bigas C, Benitah SA. The role of lipids in cancer progression and metastasis. *Cell Metab.* 2022;34(11):1675–99.
- Arner P, Bernard S, Salehpour M, Possnert G, Liebl J, Steier P, et al. Dynamics of human adipose lipid turnover in health and metabolic disease. *Nature.* 2011;478(7367):110–3.
- Kimura I, Ichimura A, Ohue-Kitano R, Igarashi M. Free fatty acid receptors in health and disease. *Physiol Rev.* 2020;100(1):171–210.
- Mu H, Hoy CE. The digestion of dietary triacylglycerols. *Prog Lipid Res.* 2004;43(2):105–33.
- Holtf M, Lenaerts C, Cullen D, Vanden BJ. Extracellular nutrient digestion and absorption in the insect gut. *Cell Tissue Res.* 2019;377(3):397–414.
- Grillo LAM, Majerowicz D, Gondim KC. Lipid metabolism in *Rhodnius prolixus* (Hemiptera: Reduviidae): role of a midgut triacylglycerol-lipase. *Insect Biochem Mol Biol.* 2007;37(6):579–88.
- Gondim KC, Atella GC, Pontes EG, Majerowicz D. Lipid metabolism in insect disease vectors. *Insect Biochem Mol Biol.* 2018;101:108–23.
- Fritzen AM, Lundsgaard AM, Kiens B. Tuning fatty acid oxidation in skeletal muscle with dietary fat and exercise. *Nat Rev Endocrinol.* 2020;16(12):683–96.

9. Ebert D, Haller RG, Walton ME. Energy contribution of octanoate to intact rat brain metabolism measured by ¹³C nuclear magnetic resonance spectroscopy. *J Neurosci*. 2003;23(13):5928–35.
10. Schott MB, Weller SG, Schulze RJ, Krueger EW, Drizyte-Miller K, Casey CA, et al. Lipid droplet size directs lipolysis and lipophagy catabolism in hepatocytes. *J Cell Biol*. 2019;218(10):3320–35.
11. Luo J, Yang H, Song BL. Mechanisms and regulation of cholesterol homeostasis. *Nat Rev Mol Cell Biol*. 2020;21(4):225–45.
12. Yang A, Mottillo EP. Adipocyte lipolysis: from molecular mechanisms of regulation to disease and therapeutics. *Biochem J*. 2020;477(5):985–1008.
13. Zechner R, Zimmermann R, Eichmann TO, Kohlwein SD, Haemmerle G, Lass A, et al. Fat signals-lipases and lipolysis in lipid metabolism and signaling. *Cell Metab*. 2012;15(3):279–91.
14. Sadurska B, Skalska-Hilgier E. Role of lipases in human metabolism. *Postepy Hig Med Dosw*. 2001;55(4):541–63.
15. Wong H, Schotz MC. The lipase gene family. *J Lipid Res*. 2002;43(7):993–9.
16. Schweiger M, Schreiber R, Haemmerle G, Lass A, Fledelius C, Jacobsen P, et al. Adipose triglyceride lipase and hormone-sensitive lipase are the major enzymes in adipose tissue triacylglycerol catabolism. *J Biol Chem*. 2006;281(52):40236–41.
17. Kumar N, Thunuguntla VB, Veeramachaneni GK, Guntupalli S, Bondili JS. Molecular characterization of human ABHD2 as TAG lipase and ester hydrolase. *Biosci Rep*. 2016;36(4):e00358.
18. Pusch LM, Riegler-Berket L, Oberer M, Zimmermann R, Taschler U. Alpha/beta-hydrolase domain-containing 6 (ABHD6)—a multifunctional lipid hydrolase. *Metabolites*. 2022;12(8):761.
19. Ma P, Zhang Y, Liang Q, Yin Y, Wang S, Han R, et al. Mifepristone (RU486) inhibits dietary lipid digestion by antagonizing the role of glucocorticoid receptor on lipase transcription. *iScience*. 2021;24(6):102507.
20. Kaltenecker D, Mueller KM, Benedikt P, Feiler U, Themanns M, Schleder M, et al. Adipocyte STAT5 deficiency promotes adiposity and impairs lipid mobilisation in mice. *Diabetologia*. 2017;60(2):296–305.
21. Hollysz M, Derebecka-Holysz N, Trzeciak WH. Transcription of *Lipe* gene encoding hormone-sensitive lipase/cholesteryl esterase is regulated by SF-1 in human adrenocortical cells: involvement of protein kinase A signal transduction pathway. *J Mol Endocrinol*. 2011;46(1):29–36.
22. Miguel-Aliaga I, Jasper H, Lemaitre B. Anatomy and physiology of the digestive tract of *Drosophila melanogaster*. *Genetics*. 2018;210(2):357–96.
23. Arrese EL, Soulares JL. Insect fat body: energy, metabolism, and regulation. *Annu Rev Entomol*. 2010;55:207–25.
24. Li YL, Yao YX, Zhao YM, Di YQ, Zhao XF. The steroid hormone 20-hydroxyecdysone counteracts insulin signaling via insulin receptor dephosphorylation. *J Biol Chem*. 2021;296:100318.
25. Jindra M, Tumova S, Milacek M, Bittova L. A decade with the juvenile hormone receptor. *Adv Insect Phys*. 2021;60:37–85.
26. Zhao XF. G protein-coupled receptors function as cell membrane receptors for the steroid hormone 20-hydroxyecdysone. *Cell Commun Signal*. 2020;18(1):146.
27. Hill RJ, Billas IM, Bonneton F, Graham LD, Lawrence MC. Ecdysone receptors: from the ashburner model to structural biology. *Annu Rev Entomol*. 2013;58:251–71.
28. Liu Y, Sheng Z, Liu H, Wen D, He Q, Wang S, et al. Juvenile hormone counteracts the bHLH-PAS transcription factors MET and GCE to prevent caspase-dependent programmed cell death in *Drosophila*. *Development*. 2009;136(12):2015–25.
29. DiAngelo JR, Birnbaum MJ. Regulation of fat cell mass by insulin in *Drosophila melanogaster*. *Mol Cell Biol*. 2009;29(24):6341–52.
30. McMullen E, Hertenstein H, Strassburger K, Deharde L, Brankatschk M, Schirmeier S. Glycolytically impaired *Drosophila* glial cells fuel neural metabolism via β -oxidation. *Nat Commun*. 2023;14(1):2996.
31. Schulz JG, Laranjeira A, Van Huffel L, Gärtner A, Vilain S, Bastianen J, et al. Glial β -Oxidation regulates *Drosophila* energy metabolism. *Sci Rep*. 2015;5(1):7805.
32. Wang XP, Huang Z, Li YL, Jin KY, Dong DJ, Wang JX, et al. Krüppel-like factor 15 integrated autophagy and gluconeogenesis to maintain glucose homeostasis under 20-hydroxyecdysone regulation. *PLoS Genet*. 2022;18(6):e1010229.
33. Li M, Mead EA, Zhu J. Heterodimer of two bHLH-PAS proteins mediates juvenile hormone-induced gene expression. *Proc Natl Acad Sci U S A*. 2011;108:638–43.
34. Shao HL, Zheng WW, Liu PC, Wang Q, Wang JX, Zhao XF. Establishment of a new cell line from lepidopteran epidermis and hormonal regulation on the genes. *PLoS ONE*. 2008;3(9):e3127.
35. Cai MJ, Zhao WL, Jing YP, Song Q, Zhang XQ, Wang JX, et al. 20-Hydroxyecdysone activates forkhead box O to promote proteolysis during *Helicoverpa armigera* molting. *Development*. 2016;143(6):1005–15.
36. Chen CH, Pan J, Di YQ, Liu W, Hou L, Wang JX, et al. Protein kinase C delta phosphorylates ecdysone receptor B1 to promote gene expression and apoptosis under 20-hydroxyecdysone regulation. *Proc Natl Acad Sci U S A*. 2017;114(34):E7121–30.
37. McGarry JD, Foster DW. Regulation of hepatic fatty acid oxidation and ketone body production. *Annu Rev Biochem*. 1980;49:395–420.
38. Edens NK, Leibel RL, Hirsch J. Mechanism of free fatty acid re-esterification in human adipocytes in vitro. *J Lipid Res*. 1990;31(8):1423–31.
39. Zechner R, Madeo F, Kratky D. Cytosolic lipolysis and lipophagy: two sides of the same coin. *Nat Rev Mol Cell Biol*. 2017;18(11):671–84.
40. Sathyanarayan A, Mashek MT, Mashek DG. ATGL promotes autophagy/lipophagy via SIRT1 to control hepatic lipid droplet catabolism. *Cell Rep*. 2017;19(1):1–9.
41. Recazens E, Mousel E, Langin D. Hormone-sensitive lipase: sixty years later. *Prog Lipid Res*. 2021;82:101084.
42. Douglass JD, Zhou YX, Wu A, Zadroga JA, Gajda AM, Lackey AI, et al. Global deletion of MGL in mice delays lipid absorption and alters energy homeostasis and diet-induced obesity. *J Lipid Res*. 2015;56(6):1153–71.
43. Huang JH, Jing X, Douglas AE. The multi-tasking gut epithelium of insects. *Insect Biochem Mol Biol*. 2015;67:15–20.
44. Ghosh A, Gao L, Thakur A, Siu PM, Lai CWK. Role of free fatty acids in endothelial dysfunction. *J Biomed Sci*. 2017;24(1):50.
45. Boden G. Effects of free fatty acids on gluconeogenesis and glycogenolysis. *Life Sci*. 2003;72(9):977–88.
46. Van der Horst DJ. Insect adipokinetic hormones: release and integration of flight energy metabolism. *Comp Biochem Physiol B Biochem Mol Biol*. 2003;136(2):217–26.
47. Kuzawa CW, Chugani HT, Grossman LI, Lipovich L, Muzik O, Hof PR, et al. Metabolic costs and evolutionary implications of human brain development. *Proc Natl Acad Sci U S A*. 2014;111(36):13010–5.
48. Mitchell RW, On NH, Del Bigio MR, Miller DW, Hatch GM. Fatty acid transport protein expression in human brain and potential role in fatty acid transport across human brain microvessel endothelial cells. *J Neurochem*. 2011;117(4):735–46.
49. Jang S, Choi B, Lim C, Lee B, Cho KS. Roles of *Drosophila* fatty acid-binding protein in development and behavior. *Biochem Biophys Res Commun*. 2022;599:87–92.
50. Dourlen P, Sujkowski A, Wessells R, Mollereau B. Fatty acid transport proteins in disease: new insights from invertebrate models. *Prog Lipid Res*. 2015;60:30–40.
51. Weiler A, Volkenhoff A, Hertenstein H, Schirmeier S. Metabolite transport across the mammalian and insect brain diffusion barriers. *Neurobiol Dis*. 2017;107:15–31.
52. Palm W, Sampaio JL, Brankatschk M, Carvalho M, Mahmoud A, Shevchenko A, et al. Lipoproteins in *Drosophila melanogaster*-assembly, function, and influence on tissue lipid composition. *PLoS Genet*. 2012;8(7):e1002828.
53. Carvalho M, Sampaio JL, Palm W, Brankatschk M, Eaton S, Shevchenko A. Effects of diet and development on the *Drosophila* lipidome. *Mol Syst Biol*. 2012;8:600.
54. Brankatschk M, Eaton S. Lipoprotein particles cross the blood-brain barrier in *Drosophila*. *J Neurosci*. 2010;30(31):10441–7.
55. Ow JR, Caldez MJ, Zafer G, Foo JC, Li HY, Ghosh S, et al. Remodeling of whole-body lipid metabolism and a diabetic-like phenotype caused by loss of CDK1 and hepatocyte division. *Elife*. 2020;9:e63835.
56. Jindra M, Palli SR, Riddiford LM. The juvenile hormone signaling pathway in insect development. *Annu Rev Entomol*. 2013;58:181–204.
57. Jindra M, Belles X, Shinoda T. Molecular basis of juvenile hormone signaling. *Curr Opin Insect Sci*. 2015;1:39–46.
58. Li YX, Wang D, Zhao WL, Zhang JY, Kang XL, Li YL, et al. Juvenile hormone induces methoprene-tolerant 1 phosphorylation to increase interaction with Taiman in *Helicoverpa armigera*. *Insect Biochem Mol Biol*. 2021;130:103519.
59. Riddiford LM. Juvenile hormone action: a 2007 perspective. *J Insect Physiol*. 2008;54(6):895–901.

60. Mirth CK, Tang HY, Makohon-Moore SC, Salhadar S, Gokhale RH, Warner RD, et al. Juvenile hormone regulates body size and perturbs insulin signaling in *Drosophila*. *Proc Natl Acad Sci U S A*. 2014;111:7018–23.
61. Hatem NE, Wang Z, Nave KB, Koyama T, Suzuki Y. The role of juvenile hormone and insulin/TOR signaling in the growth of *Manduca sexta*. *BMC Biol*. 2015;13:44.
62. Kang XL, Zhang JY, Wang D, Zhao YM, Han XL, Wang JX, et al. The steroid hormone 20-hydroxyecdysone binds to dopamine receptor to repress lepidopteran insect feeding and promote pupation. *PLoS Genet*. 2019;15(8):e1008331.
63. El-Merahbi R, Viera JT, Valdes AL, Kolczynska K, Reuter S, Löffler MC, et al. The adrenergic-induced ERK3 pathway drives lipolysis and suppresses energy dissipation. *Genes Dev*. 2020;34(7–8):495–510.
64. Peckett AJ, Wright DC, Riddell MC. The effects of glucocorticoids on adipose tissue lipid metabolism. *Metabolism*. 2011;60(11):1500–10.
65. Chakrabarti P, Kandror KV. FOXO1 controls insulin-dependent adipose triglyceride lipase (ATGL) expression and lipolysis in adipocytes. *J Biol Chem*. 2009;284(20):13296–300.
66. Wang B, Moya N, Niessen S, Hoover H, Mihaylova MM, Shaw RJ, et al. A hormone-dependent module regulating energy balance. *Cell*. 2011;145(4):596–606.
67. Vihervaara T, Puig O. dFOXO regulates transcription of a *Drosophila* acid lipase. *J Mol Biol*. 2008;376(5):1215–23.
68. Hossain MS, Liu Y, Zhou S, Li K, Tian L, Li S. 20-Hydroxyecdysone-induced transcriptional activity of FOXO upregulates *brummer* and *acid lipase-1* and promotes lipolysis in *Bombyx* fat body. *Insect Biochem Mol Biol*. 2013;43(9):829–38.
69. Zhao Y, Wang Y, Zhu WG. Applications of post-translational modifications of FOXO family proteins in biological functions. *J Mol Cell Biol*. 2011;3(5):276–82.
70. van der Heide LP, Smidt MP. Regulation of FOXO activity by CBP/p300-mediated acetylation. *Trends Biochem Sci*. 2005;30(2):81–6.
71. Brent MM, Anand R, Marmorstein R. Structural basis for DNA recognition by FOXO1 and its regulation by posttranslational modification. *Structure*. 2008;16(9):1407–16.
72. Consolaro F, Ghaem-Maghami S, Bortolozzi R, Zona S, Khongkow M, Basso G, et al. FOXO3a and posttranslational modifications mediate glucocorticoid sensitivity in B-ALL. *Mol Cancer Res*. 2015;13(12):1578–90.
73. Yoshimochi K, Daitoku H, Fukamizu A. PCAF represses transactivation function of FOXO1 in an acetyltransferase-independent manner. *J Recept Signal Transduct Res*. 2010;30(1):43–9.
74. Liu TW, Zhao YM, Jin KY, Wang JX, Zhao XF. KAT8 is upregulated and recruited to the promoter of *Atg8* by FOXO to induce H4 acetylation for autophagy under 20-hydroxyecdysone regulation. *J Biol Chem*. 2024;300(3):105704.
75. Nijhout HF, Riddiford LM, Mirth C, Shingleton AW, Suzuki Y, Callier V. The developmental control of size in insects. *Wiley Interdiscip Rev Dev Biol*. 2014;3(1):113–34.
76. Mirth C, Truman JW, Riddiford LM. The role of the prothoracic gland in determining critical weight for metamorphosis in *Drosophila melanogaster*. *Curr Biol*. 2005;15(20):1796–807.
77. Xie K, Tian L, Guo X, Li K, Li J, Deng X, et al. BmATG5 and BmATG6 mediate apoptosis following autophagy induced by 20-hydroxyecdysone or starvation. *Autophagy*. 2016;12(2):381–96.
78. Li YB, Li XR, Yang T, Wang JX, Zhao XF. The steroid hormone 20-hydroxyecdysone promotes switching from autophagy to apoptosis by increasing intracellular calcium levels. *Insect Biochem Mol Biol*. 2016;79:73–86.
79. Suzuki Y, Koyama T, Hiruma K, Riddiford LM, Truman JW. A molt timer is involved in the metamorphic molt in *Manduca sexta* larvae. *Proc Natl Acad Sci U S A*. 2013;110(31):12518–25.
80. Kang XL, Li YX, Li YL, Wang JX, Zhao XF. The homotetramerization of a GPCR transmits the 20-hydroxyecdysone signal and increases its entry into cells for insect metamorphosis. *Development*. 2021;148(5):dev196667.
81. Zhao XF, Wang JX, Wang YC. Purification and characterization of a cysteine proteinase from eggs of the cotton bollworm, *Helicoverpa armigera*. *Insect Biochem Mol Biol*. 1998;28(4):259–64.
82. Hide WA, Chan L, Li WH. Structure and evolution of the lipase superfamily. *J Lipid Res*. 1992;33(2):167–78.
83. Fuchs CD, Radun R, Dixon ED, Mlitz V, Timelthaler G, Halilbasic E, et al. Hepatocyte-specific deletion of adipose triglyceride lipase (adipose triglyceride lipase/patatin-like phospholipase domain containing 2) ameliorates dietary induced steatohepatitis in mice. *Hepatology*. 2022;75(1):125–39.
84. Shen Y, Chen G, Zhao S, Wu X. Genome-wide identification of lipases in silkworm (*Bombyx mori*) and their spatio-temporal expression in larval midgut. *Gene*. 2022;1:813.
85. Livak KJ, Schmittgen TD. Analysis of relative gene expression data using real-time quantitative PCR and the 2(-Delta Delta C(T)) method. *Methods*. 2001;25(4):402–8.
86. Zamore PD, Tuschl T, Sharp PA, Bartel DP. RNAi: double-stranded RNA directs the ATP-dependent cleavage of mRNA at 21 to 23 nucleotide intervals. *Cell*. 2000;101(1):25–33.
87. Fire A, Xu S, Montgomery MK, Kostas SA, Driver SE, Mello CC. Potent and specific genetic interference by double-stranded RNA in *Caenorhabditis elegans*. *Nature*. 1998;391(6669):806–11.
88. Xu J, Wang XF, Chen P, Liu FT, Zheng SC, Ye H, et al. RNA interference in moths: mechanisms, applications, and progress. *Genes (Basel)*. 2016;7(10):88.
89. Deng Z, Zhang Y, Li L, Xie X, Huang J, Zhang M, et al. A dual-luciferase reporter system for characterization of small RNA target genes in both mammalian and insect cells. *Insect Sci*. 2022;29(3):631–44.

Publisher's Note

Springer Nature remains neutral with regard to jurisdictional claims in published maps and institutional affiliations.